Powder Technology 449 (2025) 120364

Contents lists available at ScienceDirect

Powder Technology

journal homepage: www.journals.elsevier.com/powder-technology

Data-driven system identification and model predictive control of pneumatic conveying using nonlinear dynamics analysis for optimised energy consumption

Osamh S. Alshahed[a,*], Baldeep Kaur[a], Michael S.A. Bradley[a], David Armour-Chelu[b]

[a] Wolfson Centre for Bulk Solids Handling Technology, University of Greenwich, Kent ME4 4TB, UK
[b] School of Engineering, University of Greenwich, Kent ME4 4TB, UK.

HIGHLIGHTS

- Developed integrated nonlinear dynamics analysis, system identification and control.
- Measured electrostatic signals to capture nonlinear dynamics of gas-solid flows.
- Applied sparse identification with control to predict nonlinear dynamics measures.
- Evaluated model predictive control models to find an effective control strategy.
- Achieved significant energy reduction with efficient real-time control optimisation.

GRAPHICAL ABSTRACT

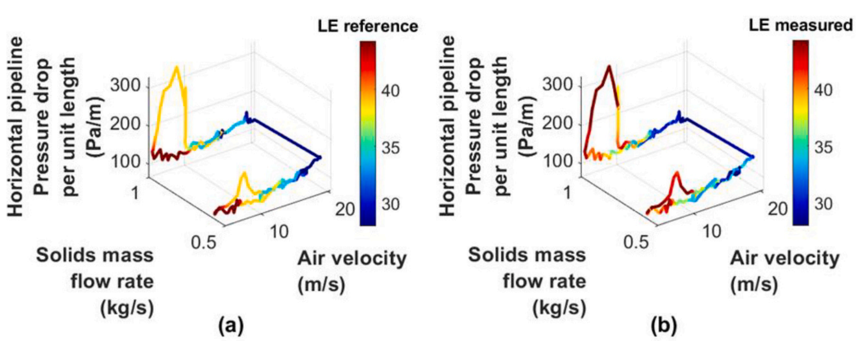

ARTICLE INFO

Keywords:
Pneumatic conveying
Chaos analysis
Recurrence quantification analysis
Sparse identification of nonlinear dynamics
Model predictive control

ABSTRACT

Pneumatic conveying systems provide secure transportation of particulate material and a dust-free environment. These systems face high energy consumption, material degradation, and pipeline blockages. This research presents an innovative solution by integrating nonlinear dynamics analysis of electrostatic sensor data, including chaos and recurrence quantification analysis, sparse identification of nonlinear dynamics with control (SINDYc) and model predictive control (MPC). The Lyapunov exponent, approximate entropy and recurrence rate of electrostatic sensor data reveal the chaotic nature of gas-solid flows. MPC framework was tailored for real-time optimisation of a pneumatic conveying system. SINDYc system models were developed using data collected from an open-loop control pneumatic conveying process to conduct MPC simulations and select an appropriate model for real-time control. This research illustrates the potential of integrating nonlinear dynamics analysis, SINDYc integrated and MPC for enhanced system performance, showcased a significant reduction in energy consumption without compromising the system's efficiency or reliability.

* Corresponding author.
E-mail address: O.Alshahed@greenwich.ac.uk (O.S. Alshahed).

https://doi.org/10.1016/j.powtec.2024.120364
Received 25 August 2024; Received in revised form 5 October 2024; Accepted 14 October 2024
Available online 16 October 2024

1. Introduction

Pneumatic conveying systems operate in three modes: dilute, transition and dense phase. Selection depends on the material properties, conveying route structure and distance, and pressure availability in the pipelines [1]. The dilute phase is characterised by high air velocity and low concentration of particulates, which ensures stable operation but can lead to energy wastage and material wear [2,3]. The dense phase is characterised by a high concentration of particulates and slower airflow, offering better product quality but demanding higher initial equipment costs due to increased pressure needs [4]. The pneumatic conveying state diagram maps the transition from dilute to dense phase for specific materials, correlating air velocity with pressure drop in a consistent pipeline diameter [5,6]. The minimum conveying air velocity (MCAV) is the optimal condition for minimum energy consumption operations, and the pressure drop minimum curve (PMC) is the line connecting the MCAV at varying solids mass flow rates. Operating near or below MCAV can risk pipeline blockages. Near the MCAV, air velocity causes uneven particle accumulation in horizontal pipelines, forming unstable dense clusters. Reducing the air velocity below MCAV intensifies these instabilities, expanding clusters and altering inner wall pressure. This affects the dilute phase, forcing it through ever-changing, restricted cross-sections.

Two main operating parameters must be designed in a pneumatic conveying system to successfully transport particulate materials in a pipeline system: the air and solids mass flow rates. The optimal values for these parameters for minimum energy consumption operations in a horizontal pipeline are revealed using the relationship between air velocity, solids mass flow rate and pressure drop in the state diagram. Although it is understood that at a constant solids mass flow rate, the relationship between air velocity and pressure has a global minimum at the MCAV, separating the dilute phase from the dense phase conveying operation, there are uncertainties in predicting its location. A small perturbation in the solids mass flow rate while operating in the dilute phase near the MCAV will increase the pressure in the pipeline. Consequently, the air velocity will decrease below the MCAV. At this stage, pipeline blockage will likely occur for dilute phase-only capable materials [7]. In contrast, the flow will be unstable for materials with dense phase conveying capabilities as they transition from dilute to dense phase conveying [5,8,9].

Consider a pneumatic conveying system that uses a linear controller, like the proportional-integral-derivative (PID), to adjust the air velocity to achieve a target pressure drop near the point of minimum pressure drop. This system will struggle to respond effectively to a sudden increase in the flow rate of solids, potentially leading to pipeline blockages. Conversely, a decrease in the solids mass flow rate can trigger a sudden rise in the air velocity, which, if not accounted for, could lead to equipment failure. The roots of these responses lie in the shifting dynamics between air velocity and pressure drop at different solids mass flow rates. Above and below the MCAV, the relationship between the air velocity and pressure drop flips from direct to indirect. As such, attempting to control the pressure drop without knowledge of the PMC's location or without a model to anticipate the nonlinearity near the PMC might not be the best strategy for reliable operation. Numerous studies have been conducted to identify effective ways of monitoring and controlling flow behaviour near the MCAV. These often employ time-series analysis techniques, analysing data from pressure sensors [10–13], electrostatic sensors [14–16], and electrical capacitance sensors [17,18].

Transition phase flow near the PMC exhibits intricate nonlinear dynamics. These can be studied using time-delay coordinate embedding through phase spaces derived from time-series data [19]. Such phase spaces, reflecting system topology, have invariant statistical features like fractal dimension, approximate entropy and largest Lyapunov exponent [20]. In addition, its dynamics are visualised using recurrence plots [21], with morphology assessed by recurrence quantification analysis [22]. The behaviour of gas-solid interactions within fluidised bed systems has been extensively investigated using chaotic invariants [23–27] and recurrence quantification analysis [28–30]. Considerable Efforts focus on understanding flow in horizontal systems via phase space visuals from pressure data [12,13,31], while other investigations aim to measure the complex dynamics of gas-solid flow in pneumatic conveying systems employing chaos theory and recurrence quantification analysis [15,16,32,33]. Phase spaces from time-series data can mirror system topology, with certain states linking more to nonlinearity [16]. Monitoring electrostatic sensor signals in horizontal pipelines offers a non-intrusive and cost-effective method, contrasting with techniques that are costly to implement and have practical limitations, such as electrical capacitance tomography [34] or particle image velocimetry [35]. However, the electrostatic sensor is limited to measuring chargeable particles in the pipeline.

Deloughry et al. investigate the performance of positive pressure pneumatic conveying control systems using a proportional-integral algorithm to manipulate air velocity in a horizontal pipeline to reach a desired saltation/dune level and time between dunes, calculated using an electrical capacitance tomography [36]. It is concluded that the proportional-integral control algorithm can be used to maintain a saltation/dune level set point. However, an instability issue is faced due to the increased dead time of the proportional-integral control system caused by the imaging reconstruction system delay and transportation delay. Moreover, other modern control techniques, such as MPC, have been applied to pneumatic conveying and drying systems to control the air mass flow rate and temperature by manipulating a blower rpm and electric heating furnace flow rate [37,38].

Control theory is the science of controlling system inputs through actuators to achieve desired measured outputs, typically aiming to optimally control system outputs with minimised effort posed on inputs [39]. Classical control of linear systems is based on the PID control technique. The disadvantage of PID controllers is their inability to handle cross-coupling effects between different inputs and outputs, leading to suboptimal control performance in multi-input and multi-output systems. According to several studies in control engineering, it has been noted that PID controllers exhibit limitations when it comes to effectively handling strongly nonlinear system responses and constraints without the utilisation of extended control methods [40]. Modern control, such as model predictive control (MPC) [39], handles constraints and multiple control objectives and can intrinsically account for various phenomena, including system time delay (dead time), non-minimum phase dynamics and instability. MPC requires models derived from first principles or a data-driven system identification method.

Data-driven system identification uses machine learning to derive models from input-output data, bypassing prior system knowledge. Its strength lies in understanding system dynamics amidst nonlinearities and uncertainties. This capability is essential for control, optimisation, fault detection, and diagnosis applications. Data-driven identification develops models from data to strategise system control, optimising diverse applications from industry to aerospace. Its precision in controlling intricate systems lets engineers design adaptive strategies from accurate data-driven models. This method not only pinpoints system issues but also offers optimisation solutions. It gathers sensor data, processes it, forms system models, and applies control theory for feedback adjustments.

There are several machine learning techniques to build data-driven models using a black-box approach, including state-space models developed using the Eigen system realisation algorithm [41], autoregressive models [42] and neural network (NN) models [43]. These techniques are bounded, suffer from overfitting, lack physical insights, and cannot generalise beyond the training data. The NN modelling method is increasingly used to represent nonlinear systems, and recently, the deep reinforcement learning approach has shown impressive results [44]. However, the NN model structure requires a large volume of training data sets, which is often a luxury. It needs high computational power to respond to abrupt changes in the system and have effective control.

Some methods develop physically interpretable linear representations of nonlinear systems, including dynamic mode decomposition with control (DMDc) and its extensions, extended DMDc [45] and wavelet-based DMDc [46]. A recently proposed method, sparse identification of nonlinear dynamics with control (SINDYc), can quickly identify interpretable nonlinear models that capture the underlying patterns in limited data while avoiding overfitting [47]. Considering limited data, a comparative study was conducted for NN, DMDc and SNDYc to compare their control performance with the MPC framework [47]. SINDy is compared with DMDc and NN in an MPC framework using different nonlinear dynamical systems, including the Lotka-Voltera, Lorenz, and F8 crusader flight control systems. SINDY results have shown more robust properties than NN, such as the ability to train a model with limited data, the sensitivity of initial parameters setting, and training and execution time. However, suppose a low amount of data is available to model a system. If the system is weakly nonlinear and has high dimensional data, DMDc would be better suited.

Reinforcement Learning is a promising control strategy, particularly for systems requiring adaptability in highly dynamic environments. However, MPC presents several key advantages in this context. MPC provides a structured approach for controlling system inputs using known dynamic models, which is crucial in pneumatic conveying systems where real-time control of gas-solid flow is essential. Its ability to optimise performance over a defined prediction horizon ensures reliable and consistent stability. In contrast, while reinforcement Learning can autonomously learn optimal strategies, it typically requires extensive training data and time to converge on a stable policy, which is an impractical scenario for real-time industrial processes that demand immediate decision-making. MPC offers transparency and interpretability in control actions, an important aspect for industrial operators, which reinforcement Learning lacks. Given these factors, MPC is a proven solution for maintaining stability and predictability in pneumatic conveying systems, especially when operating near the MCAV [48]. The adaptive nature of the MPC approach further strengthens its suitability for such applications. The model within the MPC framework can be updated in real-time to account for new conditions when the system operates outside previously modelled scenarios. This is particularly critical during transitions from dilute phase to transition phase flow conditions below the MCAV, ensuring continuous system stability and operational efficiency during these dynamic shifts.

This study integrates nonlinear dynamics analysis of electrostatic sensor data, SINDYc and MPC in a systematic framework for the real-time optimisation of pneumatic conveying systems. The goal is to minimise the power consumption of the pneumatic conveying process through a combination of an open-loop control system, data-driven modelling using SINDYc, and optimal control using MPC. The open-loop control system was developed to generate diverse electrostatic sensor data of gas-solid flow behaviour near the PMC in the state diagram, which is the optimal minimum energy consumption operation condition in a pneumatic conveying process.

Furthermore, applying nonlinear dynamics feature extraction techniques to electrostatic sensor signals, such as the largest Lyapunov exponent, approximate entropy and recurrence rate, provides insights into the complex dynamic nature of gas-solid flows, enabling more accurate and efficient control strategies. As the electrostatic sensor is limited to measuring chargeable particles, plastic pellets were used in the pneumatic conveying experiments to explore the applicability of the nonlinear dynamics analysis techniques in controlling the gas-solid flow.

The research presented in [16] indicates that the nonlinear dynamics analysis measures applied to electrostatic sensor data of horizontal gas-solid flow of plastic pellets can be used to detect whether the flow condition is above, near or below the minimum energy consumption operating conditions. The aim of the integrated real-time control system is to achieve the minimum energy consumption through reference tracking manipulation of the nonlinear dynamics analysis measures of the flow to reduce the air velocity to the MCAV condition at a constant solids mass flow rate.

The materials and methods employed are discussed in the subsequent sections, detailing the pneumatic conveying system setup, the nonlinear dynamics analysis techniques used, and the integration of SINDYc with MPC. The ability of this approach to achieve reduced energy consumption without compromising the efficiency and reliability of the pneumatic conveying process is demonstrated through rigorous experimentation and analysis.

2. Material and methods

2.1. Data-driven system identification with control framework

The sparse identification of nonlinear dynamics with control (SINDyc) is integrated with the model predictive control (MPC) in a systematic framework to optimise the power consumption of a pneumatic conveying system. Fig. 1 shows a schematic block diagram design of a real-time control system design that can switch between two subsystems: open-loop control in Region 1, highlighted in blue, and closed-loop control in Region 2, highlighted in green. Region 3, highlighted in orange, illustrates the procedure for training and selecting SINDYc models from a dataset collected from an input-output database.

The open-loop control system design in Region 1 enforces inputs to the pneumatic conveying system through manual manipulation or predefined function to generate diverse data from pressure and electrostatic sensors. The closed-loop control design in Region 2 uses MPC to provide the system with an optimised input based on a model of the system. In both cases, the input and output time-series data are saved in a database, which is then used as the foundation for subsequent analysis, modelling and control.

The output variables of the 'Pneumatic Conveying System' block are the solids mass flow rate, superficial air velocity, pressure drop per unit length of the horizontal pipeline, and the largest Lyapunov LE, AE, and RR obtained from the bottom arc-shaped electrostatic sensor data of horizontal gas-solid flow. The pneumatic conveying system has two input variables: Roots blower speed and rotary feeder speed. The rotary feeder speed is the disturbance input, and the Roots blower speed is the user-defined manipulated input or the optimised input from the closed-loop control system. The 'Input Switch' condition block allows a value for the Roots blower speed to be send to the 'Pneumatic Conveying System' block from either a user-defined manipulated input or an optimised input from the 'MPC' block.

The approach used in implementing the closed-loop control system design encompasses several steps. The process begins with implementing the open-loop pneumatic conveying control strategy using a predefined input function enforced on the system. Data from load cell sensors, pressure sensors, and bottom arc-shaped electrostatic sensors are first collected and preprocessed. The Load cell and pressure sensor data are preprocessed to calculate the pneumatic conveying state diagram, including superficial air velocity, solids mass flow rate and pressure drop in a horizontal pipeline. The bottom arc-shaped electrostatic sensors moving data window were collected and transformed into measures using nonlinear dynamics feature extraction techniques and stored in an input-output database.

Data from the 'Input-output Database' block is collected through the 'Collect Data' block. Once a certain amount of data (5 s) is stored in the input-output database, it is sent to the 'Train SINDYc Model' block to identify an initial model. The training dataset window size increases from 5 s to a specific user-defined size. When the user-defined training dataset window size is reached, the most recent training dataset window stored in the input-output database is sent by the 'Collect Data' block to the 'Train SINDYc Model' block. This is done using an if condition when the stored input-output data time reaches the user-defined time window size, and the last user-defined time window size of stored input-output

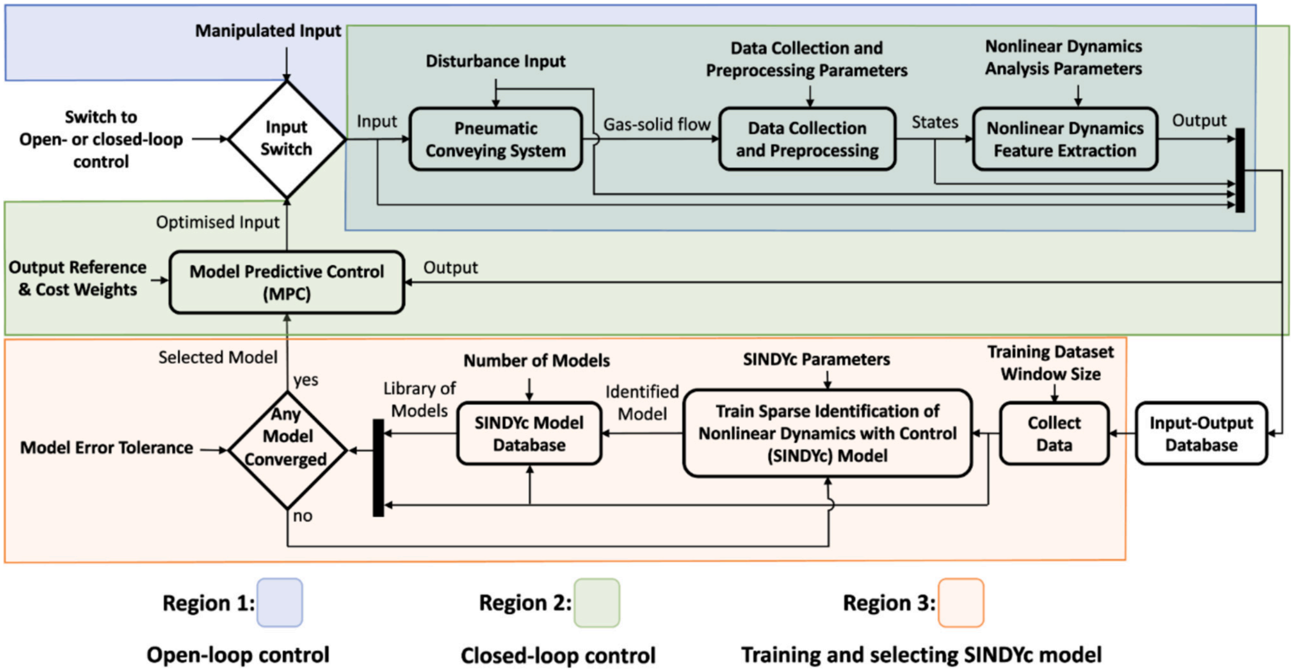

Fig. 1. A systematic framework for optimising the power consumption of a pneumatic conveying system. (a) Region 1: an open-loop control. (b) Region 2: a closed-loop control; and (3) Region 3: a procedure for selecting the MPC model from a dataset which is collected from an input-output database.

data is continuously sent to the 'Train SINDYc Model' block.

The 'Train SINDYc Model' block trains a SINDYc model from the collected dataset, which is then sent to the 'SINDYc Model Database' block to store in a library of models. The 'SINDYc Model Database' block is limited to storing a specific maximum number of SINDYc models in the model library, and it stops training new models. The library of models stored in the 'SINDYc Model Database' block is then sent to the 'Any Model Converged' if condition block. The 'Any Model Converged' block uses recently collected data from the 'Collect Data' block to calculate the mean absolute error for all the SINDYc models in the library of models to check if the error of any of the models is lower than a user-defined error tolerance. If any of the errors of the SINDYc models do not exceed the error tolerance value, the model with the minimum error is selected and sent to the 'MPC' block. At this stage, the 'MPC' block require the cost function weights and output reference value and will be ready for deployment, implemented using the open- or closed-loop control input at the 'Input Switch' condition block.

Moreover, if all the SINDYc models in the library of models have errors higher than the error tolerance value in the 'Any Model Converged' block, it sends a signal to the 'Train SINDYc Model' block to train a new model to send to the SINDYc model database. If the library of models in the SINDYc model database reaches the maximum number of models, it makes a prediction for all the stored models over the current collected dataset from the 'Collect Data' block and calculates the mean absolute error between the predictions of the models and the collected dataset. The SINDYc model database then replaces the newly trained SINDYc model in the library of models with the model with the highest error and then sends the updated library of models to the 'Any Model Converged' block.

Integrating the above steps establishes a systematic framework to optimise the output of a pneumatic conveying system in real-time by combining open-loop control for data collection, data-driven modelling using SINDYc, and optimal control using MPC. However, before applying the real-time control framework, a feature extraction technique must be selected from a set of techniques based on their control performance, which is evaluated using the MPC simulation environment framework. The sections below describe the pneumatic conveying system setup used, the SINDYc modelling method, the MPC method and the MPC simulation framework for selecting an appropriate nonlinear dynamics analysis measure for real-time MPC. LabVIEW software is used to send, collect and store data, while data preprocessing, nonlinear dynamics analysis, SINDYc modelling and MPC calculations are done using MATLAB software.

2.2. Pneumatic conveying system setup

Experiments were conducted to model and control a closed-loop industrial-scale pneumatic conveying system. Fig. 2 shows a schematic of the industrial-scale pneumatic conveying system's main components, including a pipeline cycle with a total length of 137 m and 0.1 m inner diameter, a receiving hopper and blow tank with a 1.5 m^3, a positive displacement Roots blower and a rotary feeder. The pipeline cycle has various sections, including horizontal, vertical, inclined and bends.

Ellipsoid-shaped plastic pellets with a total batch mass of 800 kg were fed to the blow tank through a feed hopper, having a mean diameter of 3.6 mm, particle density of 910 kg/m^3 and bulk density of 560 kg/m^3. The Roots blower is used to draw air at the inlet of the pipeline cycle, and then the plastic pellets were uniformly dropped from the blow tank to the conveying pipeline through the rotary feeder. At the end of the pipeline cycle, the air is separated from the plastic pellets at the receiving hopper through a bag filter house with a 35 m^2 surface area. When all the plastic pellets in the blow tank were conveyed to the receiving hopper, the Roots blower was switched off, and the process was repeated by dropping the pellets using a butterfly valve to the blow tank.

The effect of the two operating parameters was considered in studying the flow behaviour in a horizontal pipeline near the pressure drop minimum curve; the air and solids mass flow rates are the system's main input variables. Six output variables were monitored to assess the pneumatic conveying characteristics and identify the pressure drop minimum curve condition: solids mass flow rate, superficial air velocity, pressure drop per unit length of a horizontal pipeline, and the three nonlinear dynamics analysis measures extracted from the bottom arc-shaped electrostatic sensor data of horizontal gas-solid flow, including the largest Lyapunov exponent, approximate entropy and recurrence rate.

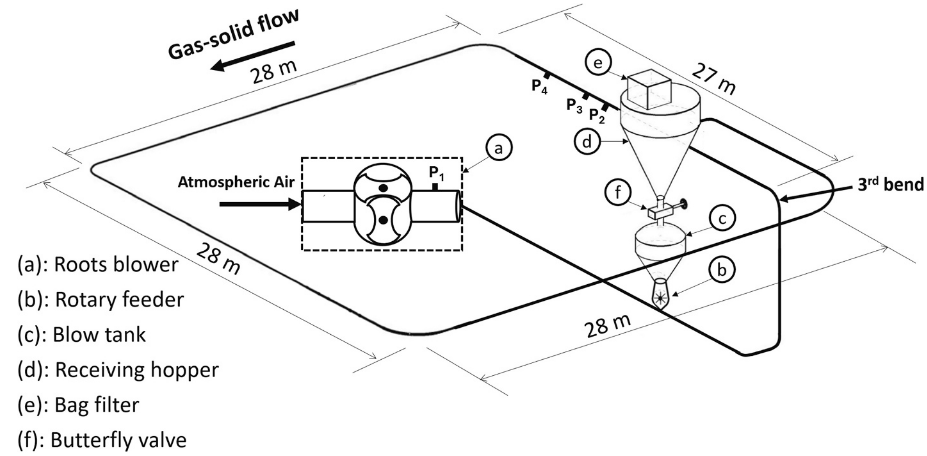

Fig. 2. A schematic of a pneumatic conveying system setup.

The Roots blower volumetric airflow is determined using a performance chart provided by Adams Ricardo Ltd. It is a 3D surface function that shows the correlation between the volumetric air flow rate, the Roots blower speed and the pressure drop from the blower's inlet pressure to its exit. Considering the airflow incompressible, the air mass flow rate can be calculated by multiplying the volumetric air flow rate by the air density, as depicted in Fig. 3 (a). The inlet airflow of the Roots blower is at atmospheric pressure, while the exit pressure, which is also the inlet of the conveying pipeline, is measured using a pressure sensor.

The solids mass flow rate is measured at the receiving hopper, which is suspended on three equidistant load cells and controlled using the rotary feeder speed at the blow tank exit. The load cells are manufactured by LCM SYSTEM LTS (STA-3-1000) with a range of up to 1000 kg and an accuracy of up to ±0.02 %. The solids mass flow rate is calculated using a linear regression fit of the measured solids mass of a fully developed flow, which varies with the rotary feeder speed. Preliminary experimental trials were conducted to create a predictive empirical model, illustrated in Fig. 3 (b). The model correlates the relationship between the rotary feeder speed and the solids mass flow rate at a constant blower speed of 1262 rpm.

Pressure measurements of gas-solid flow were undertaken using four pressure sensors manufactured by DRUCK LTD (UNIK 5000), with measurements ranging up to 50 kPa and accuracy up to ±0.04 %. The first pressure sensor ($P_{1,\text{ Blower exit}}$) is installed at the inlet of the pipeline cycle, which is also the Roots blower exit. The second sensor (P_2) is installed 10 m downstream of the third bend to ensure gas-solid flow transitions from accelerating to fully developed, as shown in Fig. 2. The third pressure sensor (P_3) is 2 m downstream of P_2, and the fourth pressure sensor (P_4) is 10 m downstream of P_3, as shown in Fig. 4. The horizontal pipeline's pressure drop per unit length is computed using linear regression fit across the three pressure sensors: P_2, P_3 and P_4. The superficial air velocity at the pressure sensor P_2 is calculated based on its value, the ambient temperature, pipeline diameter and the air mass flow rate swept by the Roots blower, assuming the airflow is an ideal gas.

The Wolfson Centre has pioneered an innovative method using an arc-shaped electrostatic sensor assembly to measure charged particles at the top and bottom sections of the pipeline [14]. Positioned at 1.62 m from the pressure sensor P2, as depicted in Fig. 4, this sensor system includes both top and bottom arc-shaped electrodes. In this research, the role of the arch-shaped electrostatic sensor assembly is to measure the electrostatic activity of charged particles at the bottom section of the horizontal pipeline using the bottom arch-shaped electrode. The bottom electrode acquires electrostatic signals, initially amplified by a trans-impedance amplifier circuit with a measurement range from −5 to +5 V. These signals are then sampled at discrete time intervals. The development of electrostatic charges on the solid particles primarily arises from collisional friction with the pipeline's inner wall, leading to continuous fluctuations between positive and negative charges. When fully charged particles pass the 100 % sensitivity zone at the bottom section of the pipeline's cross-section, the resulting voltage signals exhibit significant magnitudes before returning to zero, and this pattern repeats accordingly.

2.3. Nonlinear dynamics analysis

Several nonlinear dynamics analysis measures are utilised to characterise the behaviour of gas-solid flow systems. The primary focus is the phase space reconstruction, Lyapunov exponent, approximate entropy, and recurrence quantification analysis. Phase space reconstruction employs the time-delay coordinate embedding method, which converts a

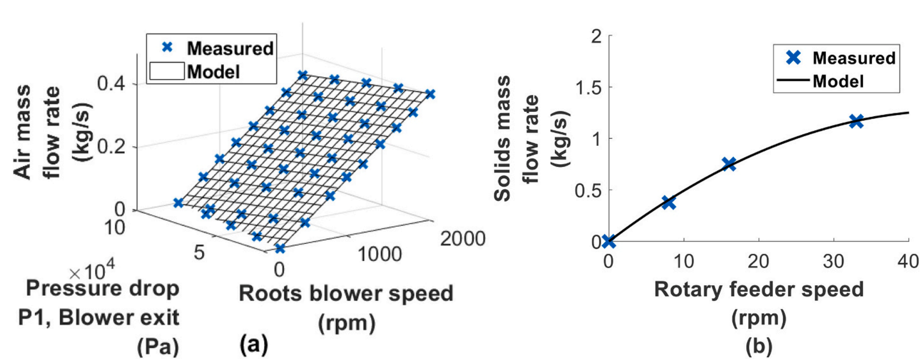

Fig. 3. (a) The Roots blower characteristic chart as a function of blower exit pressure drop, Rotors speed and air mass flow rate at constant pipe diameter of 0.1 m (b) measured mass flow rate of solids at different rotary feeder speeds and its predictive model.

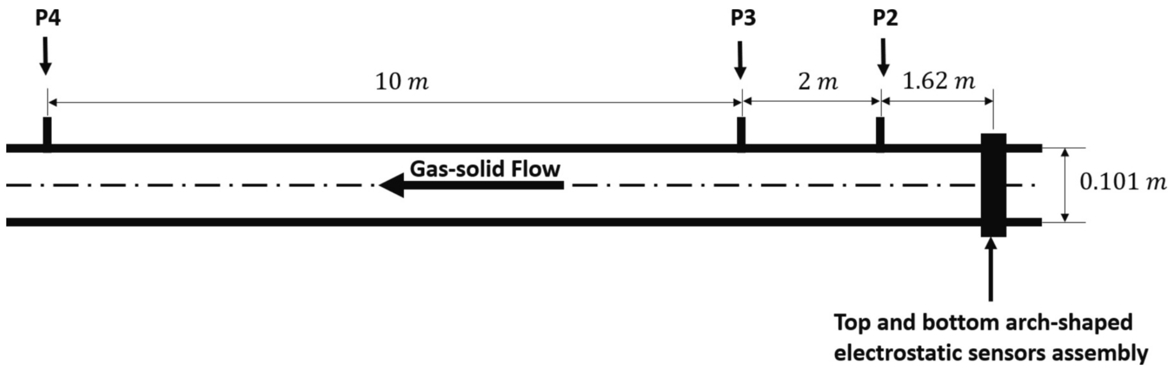

Fig. 4. Schematic diagram of the horizontal pipeline downstream of the third bend showing the location of the pressure sensors P2, P3 and P4 and the top and bottom arc-shapes electrostatic sensors assembly.

time-series signal into a vector of latent state variables. This method allows the reconstruction of a phase space that reveals topological equivalence to the original system state space, facilitating system dynamics analysis [19]. Phase space reconstruction requires parameters such as time delay and embedding dimension. Given a time series signal, a phase space can be constructed in which the system's state at different time points is represented in a high-dimensional space.

The sensitivity of initial conditions, a characteristic of chaotic behaviour, is quantified using the Lyapunov exponent. The Lyapunov exponent measures the rate at which two nearby trajectories in phase space diverge or converge. There are as many Lyapunov exponents as dimensions in a phase space. If all exponents are negative, trajectories converge, indicating stability. Conversely, positive exponents denote divergence and instability. For chaotic systems, at least one positive Lyapunov exponent signifies chaotic behaviour. The largest Lyapunov exponent is calculated using the algorithm by Rosenstein [49], as shown in Eq. 1. The LE calculation evaluates the divergence of phase points over an expansion step. The results are averaged across all phase points to provide a single value through linear regression. k_{max} and k_{min} are the minimum and maximum values of the expansion range, $\|Y_{i+k} - Y_{s+k}\| / \|Y_i - Y_s\|$ is the distance between each phase point i and its nearest neighbour s, and dt is the time step.

$$\lambda(i) = \frac{1}{k_{max} - k_{min} + 1} \sum_{k=k_{min}}^{k_{max}} \frac{1}{k \times dt} ln \frac{\|Y_{i+k} - Y_{s+k}\|}{\|Y_i - Y_s\|} \tag{1}$$

The Approximate Entropy (AE), developed by Pincus [50], assesses the unpredictability of time-series data. AE is beneficial for its low computational cost and robustness against noisy data. AE is computed by comparing the closeness of trajectories in phase space, as outlined in Eqs. 2 and 3. A lower AE indicates more predictable behaviour, while a higher AE suggests greater complexity. Φ_m and Φ_{m+1} are statistical functions computed for dimensions mmm and $m+1$, respectively, and Θ is the Heaviside function.

$$\mathrm{AE} = \Phi_m - \Phi_{m+1} \tag{2}$$

$$\Phi_m = \frac{1}{N} \sum_{i=1}^{N} log\left(\sum\nolimits_{j=1, j \neq i}^{N} \Theta\left(r - \|Y_i - Y_j\|\right) \right) \tag{3}$$

Recurrence quantification analysis provides insight into the system's structural complexity by examining the patterns of recurring dynamics within the phase space. Recurrence plots visualise recurring dynamics in phase space [51], as shown in Eq. 4, where r is the threshold hypersphere radius. The recurrence rate (RR) is the ratio of recurrent points to the total number of points, as shown in Eq. 5, developed by Zbilut and Webber [22] and Webber and Zbilut [52], highlights the frequency and duration of recurring states within the system.

$$RP_{i,j}(r) = \Theta\left(r - \left\| \overrightarrow{Y}_i - \overrightarrow{Y}_j \right\| \right) \tag{4}$$

$$RR = \frac{1}{N^2} \sum_{i=1}^{N} \sum_{j=1}^{N} RP_{i,j} \tag{5}$$

2.4. Sparse identification of nonlinear dynamics with control

Sparse identification of nonlinear dynamics with control (SINDYc) is a data-driven approach that has gained significant attention in recent years due to its ability to identify the underlying dynamics of nonlinear systems [47]. SINDYc uses a sparsity-promoting optimisation algorithm to identify a sparse set of equations of a dynamical system that balances the trade-off between complexity and prediction error. The approach begins by defining the nonlinear dynamical system as a set of differential equations, as shown in Eq. 6, where $\mathrm{f}(\mathrm{x}, \mathrm{u})$ is a function that describes the system dynamics by evolving the system from initial states to the future state while being subjected to a control input u.

$$dx/dt = \mathrm{f}(\mathrm{x}, \mathrm{u}) \tag{6}$$

The SINDYc algorithm starts by collecting the state X and control input U data snapshots from a system under study, typically in time-series data form, represented in vectors with n snapshots, as shown in Eq. 7.

$$\mathrm{X} = [\mathrm{x}_1 \ \ \mathrm{x}_2 \ \ \cdots \ \ \mathrm{x}_n], \mathrm{U} = [\mathrm{u}_1 \ \ \ \mathrm{u}_2 \ \ \ \cdots \ \ \ \mathrm{u}_n] \tag{7}$$

This data is then preprocessed by constructing a library of candidate functions $\Theta(\mathrm{X}, \mathrm{U})$ that could describe the nonlinear dynamics of the system. The candidate functions are typically chosen from a predefined set of functions, such as polynomial and trigonometric functions. Eq. 8 shows the library $\Theta(\mathrm{X}, \mathrm{U})$ using polynomial functions, where $(\mathrm{X} \bigotimes \mathrm{X})$ is the function of unique product combinations of X, $(\mathrm{X} \bigotimes \mathrm{U})$ contain unique product combinations between X and U, and q is the maximum order number to consider in the library.

$$\Theta(\mathrm{X}, \mathrm{U}) = \left[1 \quad \mathrm{X}^{\mathrm{T}} \quad \mathrm{U}^{\mathrm{T}} \quad (\mathrm{X} \bigotimes \mathrm{X})^{\mathrm{T}} \quad (\mathrm{X} \bigotimes \mathrm{U})^{\mathrm{T}} \quad \cdots \quad (X^q \bigotimes U^q)^{\mathrm{T}} \right] \tag{8}$$

The differential equation in Eq. 9 can then be reformulated to be a linear combination of nonlinear functions with sparse coefficients, as shown in Eq. 9, where $\Xi(\xi)$ is a matrix function of sparse coefficients ξ that correspond to the nonlinear terms in the library $\Theta(\mathrm{X}, \mathrm{U})$.

$$dX/dt = \Xi(\xi)\ \Theta(\mathrm{X}, \mathrm{U})^{\mathrm{T}} \tag{9}$$

The derivatives dX/dt are computed from the collected state measurements using a numerical differentiation scheme when the data is relatively smooth, such as the central difference scheme. If the data is noisy, then the total variation regularised derivative [41] will better approximate dX/dt. The sparsity-promoting regression optimisation problem in SINDYc, described in Eq. 10, ensures that the resulting set of equations is as simple and concise as possible, involving the minimum set in the vector coefficients ξ in the library $\Xi(\xi)$ necessary to describe the data accurately. The subscript k in dX_k/dt and ξ_k is the row index in dX/dt and $\Xi(\xi)$.

$$\text{Minimise}\xi_k = \text{Minimise}\left(\frac{1}{2}\|dX_k/dt - \widehat{\xi}_k\Theta(X,U)^T\|_2^2 + \varepsilon\|\widehat{\xi}_k\|_1\right) \tag{10}$$

The first term $\frac{1}{2}\left\|\dot{X}_k - \widehat{\xi}_k\Theta(X,U)^T\right\|_2^2$ of the optimisation problem enforces that the model is accurate by minimising the difference between two consecutive state measurements. The second term $\varepsilon\|\widehat{\xi}_k\|_1$ promotes sparsity as it has the L1-norm penalty on the coefficient vector $\widehat{\xi}_k$, which means that the resulting set of equations involves only a small number of terms. The parameter ε is a positive constant selected to balance model accuracy with complexity. The optimisation problem of the right-hand side term can be solved either using the least absolute shrinkage and selection operator algorithm [53] or the sequentially thresholded least square algorithm [54].

2.5. Model predictive control

Model predictive control (MPC) is a powerful reference tracking method for controlling nonlinear systems. MPC aims to optimise control input over a future horizon using a mathematical model of the system to reach a desired reference state while satisfying constraints on the control input and system state. The MPC modelling method used in this research does not account for any constraints to understand the outcome of tracking a desired state on the optimised control input. In this study the optimised control input is the Roots blower speed used to manipulate the airflow, and the desired state is a nonlinear analysis measure.

MPC has two main components: an optimiser and a predictor, as shown in Fig. 5 in a block diagram. The predictor requires a model to predict future states given a sequence of inputs. At the same time, the optimiser uses the predictor in an iterative process to optimise a sequence of inputs by minimising a predefined cost function. MPC outputs only the first control input to the existing system, and then the optimisation process is repeated in the next step. The optimiser employed within the MPC framework is nonlinear, owing to the nature of the model used. Specifically, the Sequential Quadratic Programming method available in MATLAB's nlmpc toolbox was utilised.

The cost function $J(x_{j,k}, u_{j,k})$ can be expressed as:

$$J(x_{j,k}, u_{j,k}) = L(x_{j,k}) + V(u_{j,k}) \tag{11}$$

$x_{j,k}$ and $u_{j,k}$ are the state and control input of future horizon values, where the subscripts j and k refer to the current and future values. The function $J(x_{j,k}, u_{j,k})$ includes a combination of two terms, $L(x_{j,k})$ penalises deviations of the system state from the desired reference state, and $V(u_{j,k})$ penalises the control input effort required to reach the reference state.

$$L(x_{j,k}) = \sum_{k=1}^{H_p}\left[(x_{j,k} - r_{j,k})^T W_x (x_{j,k} - r_{j,k})\right] \tag{12}$$

$$V(u_{j,k}) = \sum_{k=2}^{H_c}\left[(u_{j,k} - u_{j,k-1})^T W_u (u_{j,k} - u_{j,k-1}) + (u_{j,k})^T W_{du}(u_{j,k})\right] \tag{13}$$

H_p and H_c are the prediction and control horizon steps. W_x, W_u, and W_{du} are the optimisation weights for the state deviation, control effort for input and input rate of change. These weights are tweaked to achieve the desired performance criteria.

2.6. Model predictive control simulation framework

The control simulation framework used in this study provides a simulation environment that evaluates the performance and sensitivity of model predictive control (MPC) on a system model, as shown in Fig. 5. It iteratively applies the optimisation algorithm in MPC at each time step to update the control input based on the previous control input and current simulated system output. The MPC simulation framework may also support sensitivity analysis, where control parameters are varied to study their effects on the control system's behaviour. By systematically modifying these parameters and observing the resulting system responses, one can gain insights into the robustness and sensitivity of the MPC algorithm.

The framework requires two data-driven models to simulate a closed-loop control system. Model A and B. Model A is developed to represent the physical system, describing the effect of control and disturbance inputs on the system output. In contrast, Model B only describes the effect of control input on the system output. The disturbance input effect on the system output in Model A is not included in Model B to evaluate and understand their effects on the MPC manipulated input action and system response.

The MPC optimisation weights are all kept constant except for the weight of the input rate of change (W_{du}). The MPC simulation

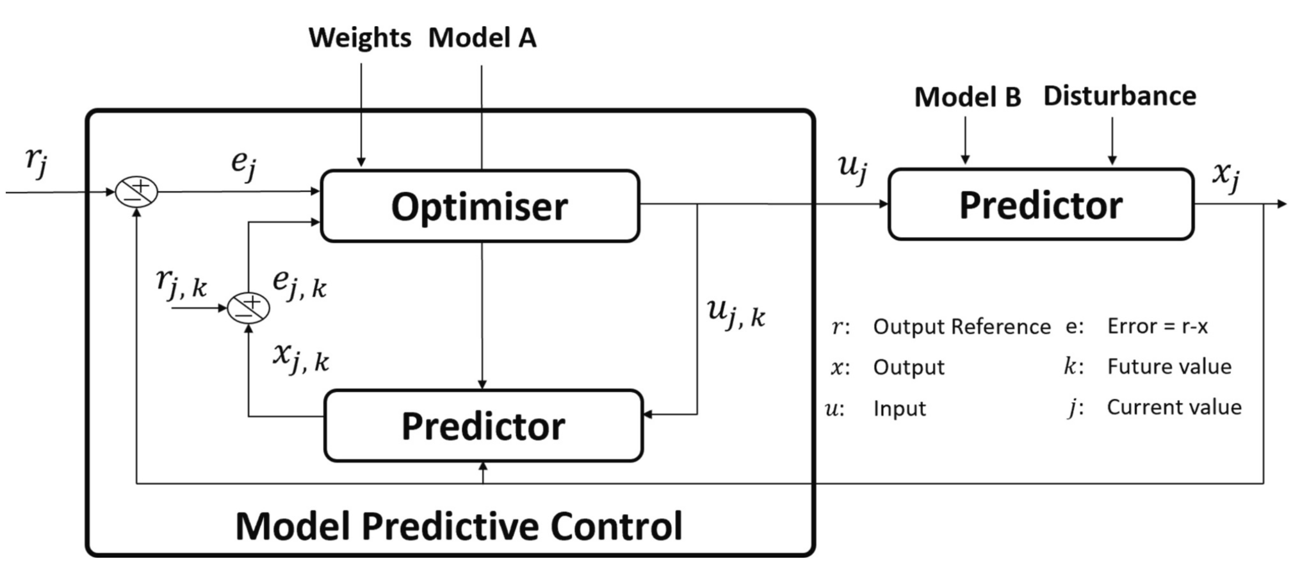

Fig. 5. Model predictive control simulation environment diagram.

framework is used in an iterative process to select the appropriate value of W_{du} and compare the control performance of different MPC models. The control performance parameters considered when comparing different MPC models are the rise time due to a step in the output reference and output overshoot peak % due to a step in the disturbance input. The algorithm used to optimise the value of W_{du} is presented in Fig. 6. The algorithm starts by applying the MPC simulation framework presented in Fig. 5, which requires a system model, an output reference and disturbance input data and an initial value for the W_{du}. The MPC simulation framework generates input-output response data, which is used to calculate the rise time and output overshoot peak %. The output overshoot peak % value is used in an if condition function to check if it falls below 10 %. If this condition is true, then the current value of W_{du} will be selected. If the output overshoot peak % is higher than 10 %, the current value of W_{du} will be increased by 1, and the MPC simulation framework will be initiated again to generate new input-output response data with the new value of output overshoot peak %.

3. Results and discussion

This research unfolded in a systematic progression of objectives to model and control gas-solid flow in pneumatic conveying of plastic pellets. Initially, the focus was on developing an open-loop pneumatic conveying control system that efficiently collects input-output data and operates the system above, near, and below the minimum conveying air velocity (MCAV). Once collected, features were extracted from the electrostatic sensor data using nonlinear dynamics analysis measures, providing valuable insights into the complex flow behaviour near the MCAV. Moreover, another dataset was collected using predefined functions of the system inputs, explicitly designed to identify models using the sparse identification of nonlinear dynamics with control (SINDYc). These models were evaluated using a model predictive control (MPC) simulation framework to assess their control performances and response to disturbance effects. This process led to the selection of an appropriate nonlinear analysis method to apply a closed-loop control system in the real-time environment developed using an MPC integrated with SINDYc. Finally, real-time MPC control case studies were conducted to investigate the control performance of the selected system model near the MCAV condition and identify potential areas for improvement, examining the impact of different control parameters.

The four sections below present the results and discussion on the objectives mentioned above. Subsection 3.1 shows the results of the open-loop control system used to identify the MCAV condition. Subsection 3.2 presents the MPC simulation case studies, which involve acquiring a dataset of the open-loop control of the flow system, developing SINDYc models from the dataset and evaluating the control performance and effect of disturbance on the developed models. Subsection 3.3 focuses on the closed-loop control case studies near the MCAV conditions, and Subsection 3.4 provide a general discussion of the results.

3.1. Open-loop control crossing the minimum conveying air velocity

The open-loop control system, shown in Fig. 1, was applied to the pneumatic conveying system to identify the operating parameter values at an optimal minimum energy consumption operation condition. This approach facilitated the collection of a dataset consisting of enforced inputs and measured outputs directing the system across the minimum conveying air velocity (MCAV). The primary purpose of identifying the system parameters at the MCAV condition is to design different control strategies that target operating conditions above, near, and below the MCAV.

Implementing the open-loop control subsystem requires parameters for data collection, preprocessing and the nonlinear dynamics analysis measures. The data collection parameters are the input frequencies of the blower and rotary feeder speeds and sampling frequencies for pressure sensors and the bottom arc-shaped electrostatic sensor. The pressure sensor data was collected at 4 Hz, while the electrostatic sensor data was collected at 100 Hz. The Roots blower speed input was manipulated at 100 Hz.

The largest Lyapunov exponent (LE), approximate entropy (AE), and recurrence rate (RR) measures were calculated from the collected bottom arc-shaped electrostatic sensor data. These measures are processed using a 10s moving window of data with a moving window step of 2.5 s, generating signals at the same rate as the open-loop control. A phase space is reconstructed for each moving window of the electrostatic sensor data window. The phase space reconstruction parameters, including time delay and embedding dimension, are set to constant values 1 and 2, respectively. The parameter required to calculate LE is the expansion range of the average log divergence function, set from 1 to 5 steps. The parameters for AE and RR are radius thresholds. The threshold hypersphere radius r for the AE measure is estimated using the 30 % standard deviation of the measurement data moving window, while the threshold hypersphere radius r value used to develop recurrence plots and calculate the RR measure is taken as a constant of 0.1.

The primary objective of this open-loop control system experiment was to identify the MCAV at which the pressure drop in a horizontal pipeline reaches its minimum while maintaining a constant solids mass flow rate of 0.56 kg/s. The control scenario for identifying the MCAV involved manual manipulation of the Roots blower rpm while keeping the solids mass flow rate at a constant value. This open-loop control scenario was designed to commence at a constant Roots blower speed of

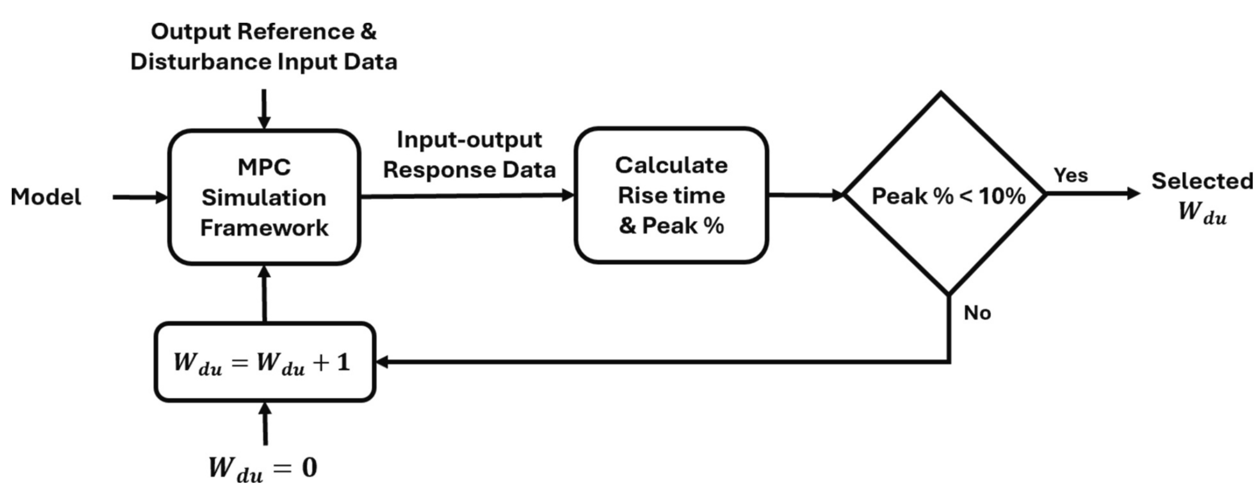

Fig. 6. The block diagram of the algorithm used to optimise the value of the MPC weight of the input rate of change (W_{du}).

1262 rpm, operating the system at a high air velocity. The speed was then sequentially stepped down by 128 rpm for four steps, starting from 1262 rpm to 746 rpm. Therefore, the time for each step was progressively increased to allow the flow to reach a steady state condition, starting from 14 s at the initial rpm of 1262, followed by 21 s, 28 s, 65 s, and 63 s.

The data from this experiment is presented in four distinct charts, as shown in Fig. 7, each representing a different variable along the y-axis. Fig. 7 (a) illustrates the rpm of the Roots blower rotors. Fig. 7 (b) presents data from the four pressure sensors, blower exit pressure, and pressure points P2, P3 and P8 in the horizontal pipeline. Fig. 7 (c) depicts the air velocity at P1 in the horizontal pipeline. Fig. 7 (d) shows the horizontal pipeline's linear pressure drop per unit length across P2, P3, and P8. The minimum pressure drop in the horizontal pipeline was recorded at 68.2 Pa/m. This value was reached during the third step down, indicating that the MCAV lies within the air velocity range of 5.9 to 8.75 m/s.

Fig. 8 shows three plots for the time-series values of the LE, AE and RR for the bottom arc-shaped electrostatic sensor. The LE time series has an inverse relationship with air velocity when operating at air velocity higher than the MCAV range, while the AE and RR have a direct relationship with air velocity. At the start of the MCAV range, the AE and RR decreased with the air velocity to a local minimum value of 0.7 and 0.0109. At the end of this MCAV range, the AE and RR measures transition to slightly higher values of 0.77 and 0.0161, respectively. The LE measure within the MCAV range keeps increasing from 39 to 45.

3.2. Model predictive control simulation of nonlinear dynamics analysis

Applying nonlinear dynamics analysis measures developed from electrostatic signal data can characterise the fully developed gas-solid flow's nonlinear dynamics and chaotic behaviour [16]. This study further explores this concept, incorporating the largest Lyapunov exponent (LE), approximate (AE), and recurrence rate (RR) measures. These measures serve as system models investigating their effectiveness in controlling the horizontal gas-solid flow of plastic pellets near the pressure minimum drop curve. The subsequent sections elaborate on the data acquisition, preprocessing, and analysis parameters for the open-loop control system used to collect a dataset and develop SINDYc models. The SINDYc models output the LE, AE, and RR measures of

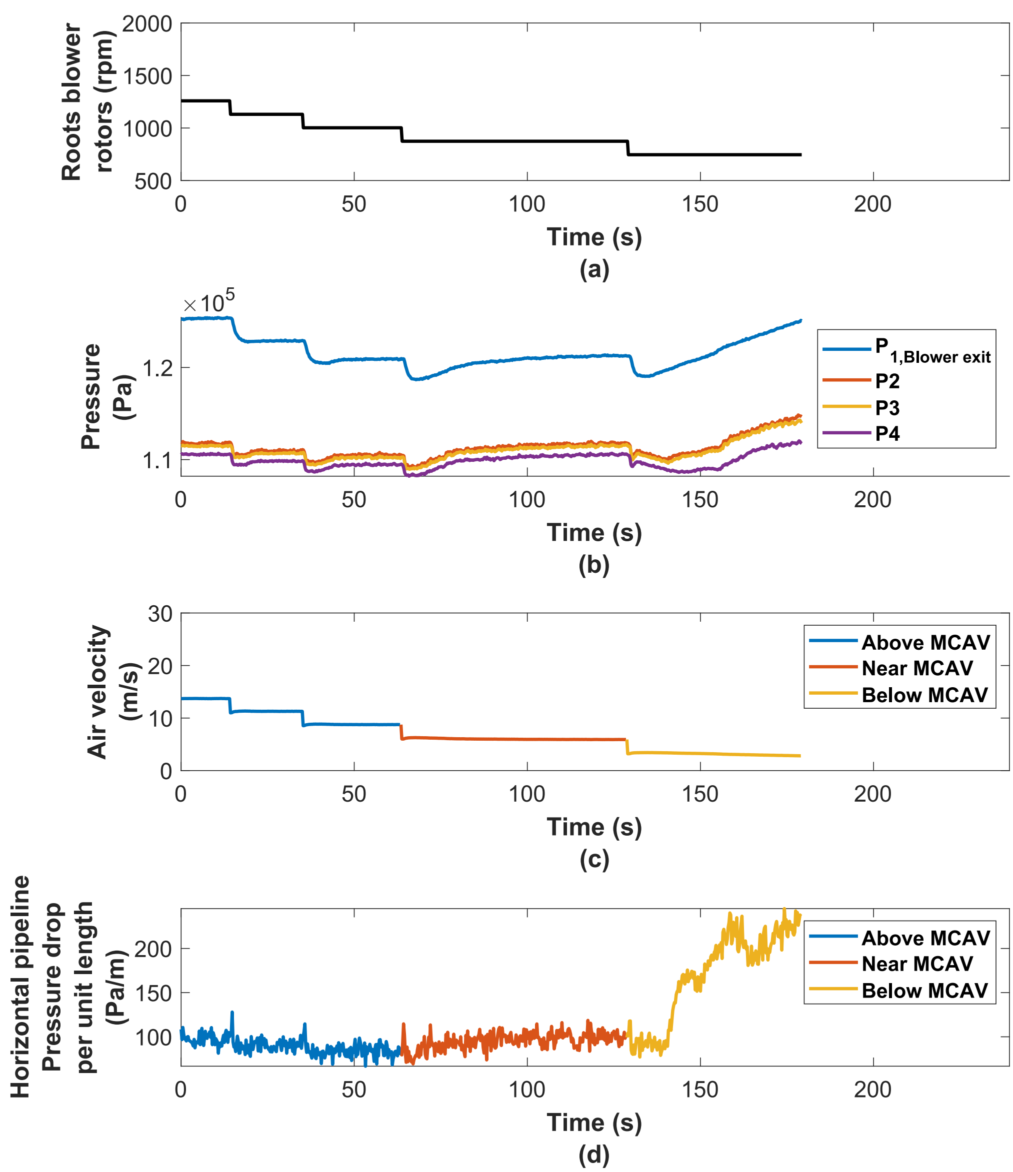

Fig. 7. (a) Roots blower speed, (b) pressure, (c) air velocity, and (d) pressure drop per unit length of the horizontal pipeline, classified into three regions above, near and below the MCAV.

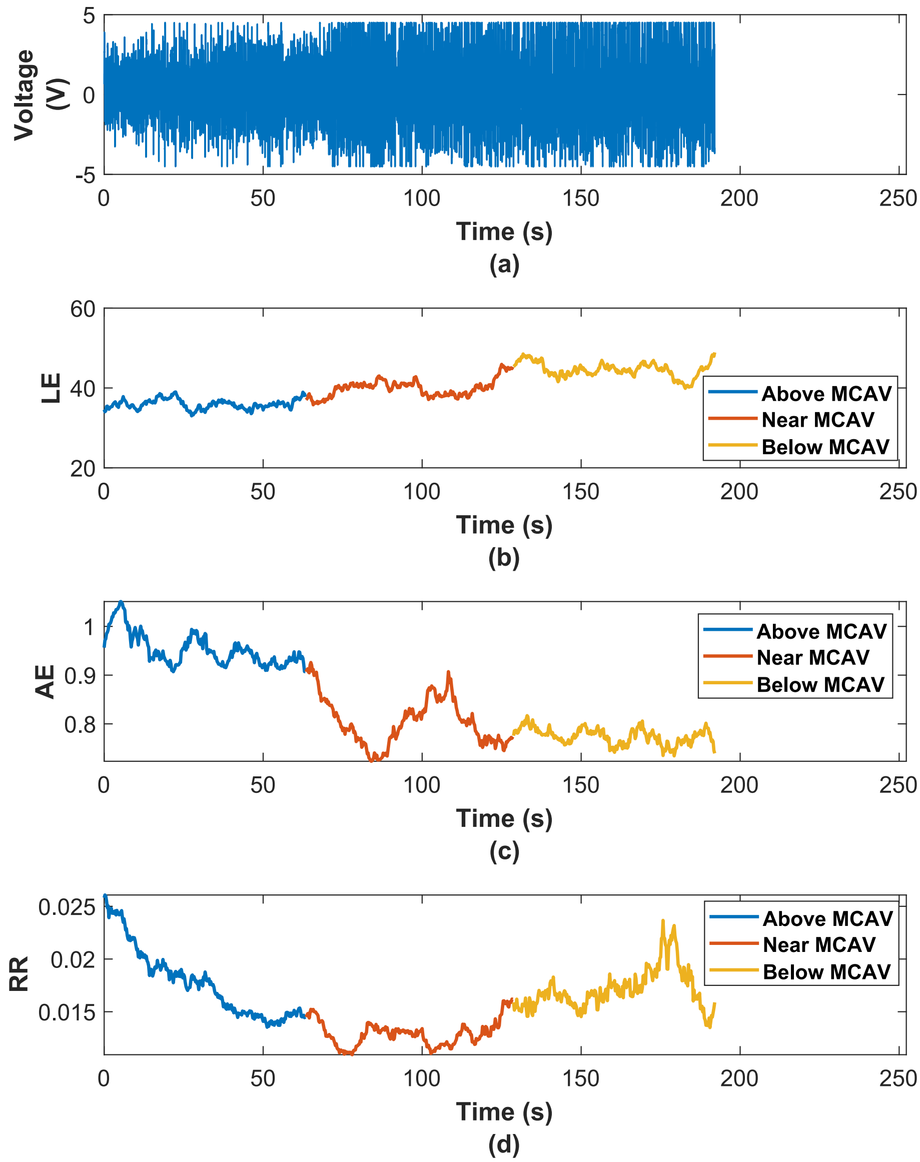

Fig. 8. Time-series representation of the data gathered from (a) bottom arc-shaped electrostatic sensor and corresponding (b) LE, (c) AE, and (d) RR measures of the above, near and below MCAV.

electrostatic signals, and the Roots blower speed and solids mass flow rate are considered inputs. In addition, they evaluate the control performance of each model incorporated in the MPC simulation framework to select the most suitable model for implementation in the real-time control design.

The dataset acquisition process was developed to ensure synchronisation between the system control inputs and the data acquired from the pressure sensors, recorded at 2 Hz. The electrostatic sensor data is collected at a higher frequency of 500 Hz and then synchronised with the control inputs by adjusting the moving data window step to 0.5 s, ensuring seamless data integration from different sources. The LE, AE, and RR parameter settings align with the description provided in Subsection 3.1.

The acquired dataset contains small and large-scale input-to-output responses of the pneumatic conveying open-loop control system. Large-scale sinusoidal wave function and small-scale Schroeder phased harmonic sequence function [55] were employed to manipulate the Roots blower speed. In addition, a square function was applied to the solids mass flow rate to evaluate its effects on the nonlinear dynamics analysis measures.

The dataset is divided into three stages, each lasting for 210 s and culminating at 630 s, as shown in Fig. 9 (a). The first stage involves manipulating the Roots blower speed using sinusoidal waves and SPHS functions for the initial 40s. The full-form SPHS function comprises ten harmonics in the sequence, repeating every 20s, and operates from 200 rpm to 1194 rpm. The sinusoidal wave has a period of 60s, centred at 1175 rpm, with lower and upper limits of 860 rpm and 1499 rpm, respectively. After the initial 40s, the SPHS and sinusoidal wave functions are applied simultaneously for the next 130 s. Following this, the sinusoidal wave function is halted, and the SPHS function continues for an additional 4 s, bringing the total duration of the first stage to 210 s. The three stages share the same manipulated input function, but the mass flow rates of solids differ. In the first stage, the solids mass flow rate is kept constant at 0.56 kg/s, increased to 1 kg/s for the second stage, and reduced to 0.56 kg/s in the third stage, as shown in Fig. 9 (b).

At the solids mass flow rate of 0.56 kg/s, the air velocity reached a minimum of 4.2 m/s in the first stage, slightly lower than the MCAV range recorded before, between 5.9 and 8.75 m/s. The pneumatic conveying system is continuously enforced on both small and large scales, preventing the air velocity and pressure drop from reaching a

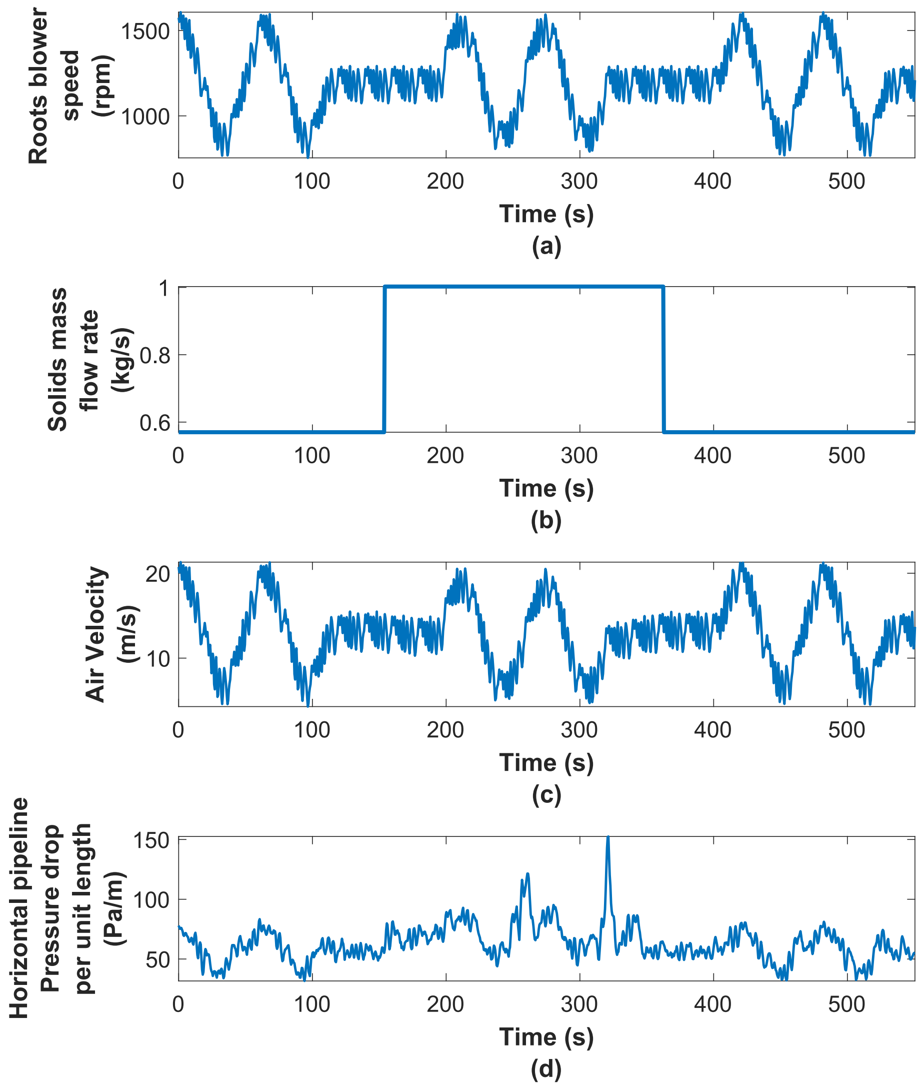

Fig. 9. Demonstration of the open-loop control system enforced inputs (a) Roots blower speed and (b) solids mass flow rate and measured horizontal pneumatic conveying states (c) air velocity and (d) pressure drop per unit length of horizontal pipeline.

steady-state condition. This approach is crucial in capturing the nonlinear dynamics analysis measures of the bottom arc-shaped electrostatic sensor under varying unstable operating conditions, providing a comprehensive understanding of its dynamic behaviour.

3.2.1. *SINDYc modelling of nonlinear dynamics analysis measures*

The sparse identification of nonlinear dynamics with control (SINDYc) method has been employed to construct three distinct system models. These models encapsulate the nonlinear dynamics analysis measures of electrostatic sensor data processed, as illustrated in Fig. 10. Each model incorporates two inputs: the Roots blower rpm and the solids mass flow rate. Despite sharing the same inputs, the models differ in their outputs: LE, AE, and RR. The structure of these models is designed such that each one represents one of the analysis measures as an output, thereby enabling the separate evaluation and differentiation of their responses.

The SINDYc algorithm is a three-step process for developing a model. The initial step involves the construction of a library of candidate functions capable of describing the behaviour observed in the input-output data. This library is designed with polynomial multiplication functions of order two of all compensation between input and output. The subsequent step is the computation of the output derivatives. Given the relative smoothness of the data, a central difference scheme is employed for this computation. The final step involves solving a sparsity-promoting regression optimisation problem. This step necessitates the parameter ε, which is selected based on the desired balance between model accuracy and complexity. The three models representing LE, AE, and RR outputs were developed with an $\varepsilon = 0.01$.

The future time stepping of the LE, AE, and RR system models is resolved using the Runge-Kutta-Fehlberg 45 method, and their predictions are showcased in Fig. 10. Statistical measures, including the mean absolute percentage error and the coefficient of determination (R-squared), were computed for each of the three models' predicted and measured data to assess model accuracy. The LE model demonstrates the lowest mean absolute percentage error of 1.4 % and the highest R-squared = 0.88. In contrast, the RR model records the highest mean absolute percentage error of 11.8 %, and the AE model has the lowest R-squared = 0.62.

3.2.2. *Model predictive control performance evaluation*

A simulation strategy is implemented to evaluate the MPC performance using the developed models describing the relationship between the blower speed and solids mass flow rate as inputs and the LE, AE and RR measures. Each model's output reference step response and disturbance step response are gathered. The simulation is conducted over 81 s, with the first 10s at minimum values for the output reference and

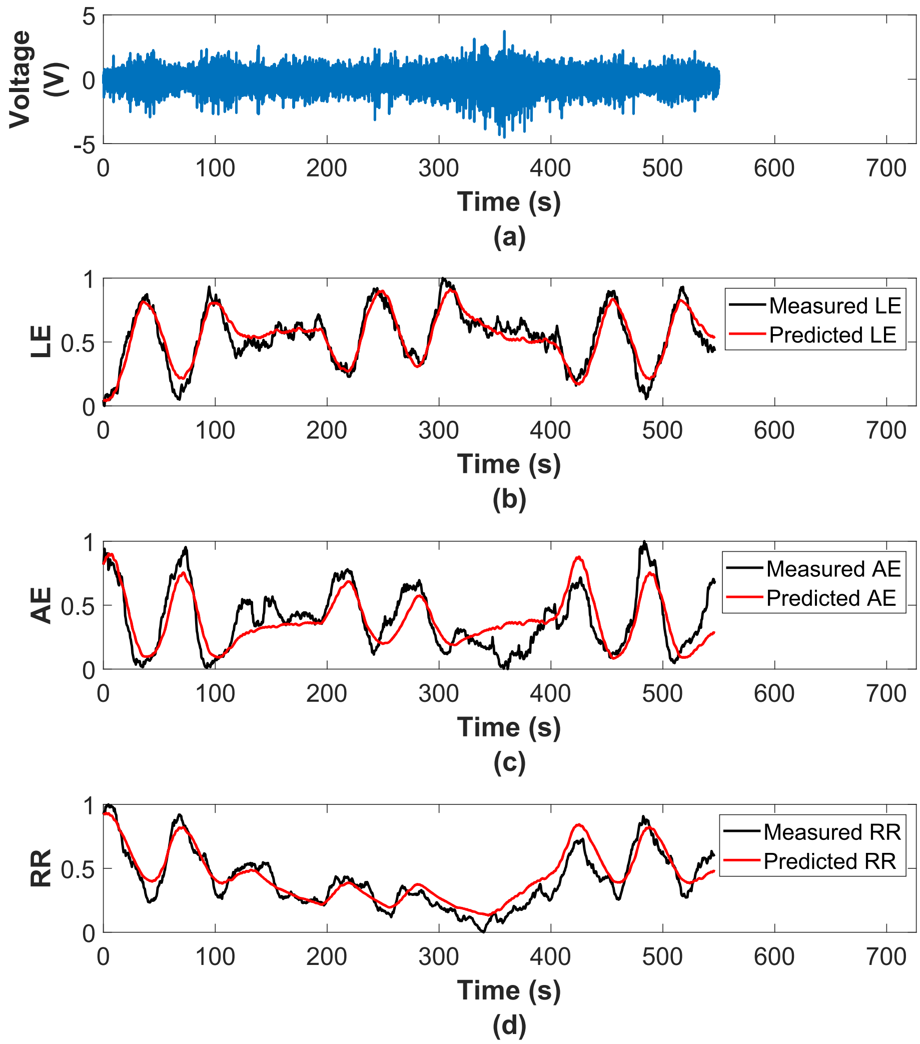

Fig. 10. (a) The bottom arc-shaped electrostatic sensor measurement and the nonlinear dynamics analysis measures, including the (b) LE, (c) AE, and (d) RR, alongside their SINDYc system model predictions.

disturbance input (solids mass flow rate). For the next 40s, the output reference is stepped up to its maximum value while the disturbance input remains constant. In the final 400 s, the disturbance input increases to its maximum value while the output reference is kept constant. This strategy is applied to each model with varying MPC optimisation weight of the input rates of change W_{du}, ranging from 5 to 30, while keeping the MPC weight for state deviation at 1, and the weight for effort of input at 0, as shown in Fig. 11 (a) and (b). The performance is evaluated based on the rise time and peak percentage for the output reference step response. In this context, the rise time is defined as the duration for the output response to elevate from 10 % to 90 % of the range from initial to steady-state value.

The parameters are selected and evaluated across a range of W_{du} values to compare the performance across different models and choose

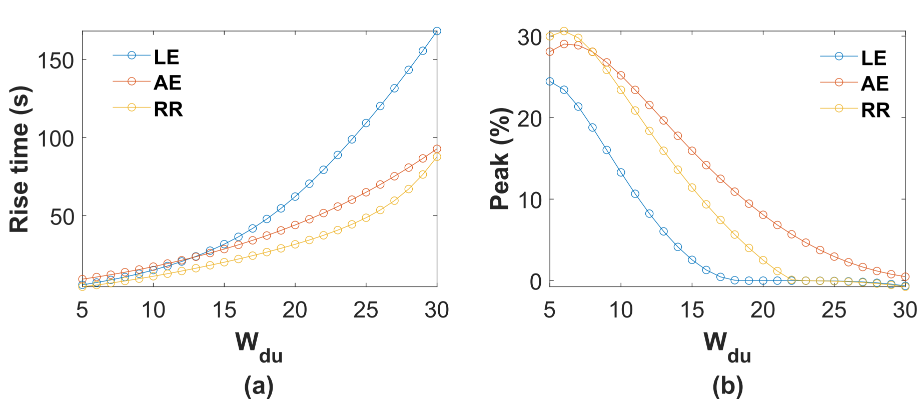

Fig. 11. (a) The rise time versus MPC cost function wight W_{du} for the LE, AE, and RR models' step responses. (b) The peak overshoot percentage for each model at $W_x = 1$ and Wu = 0.

the one with optimum control performance. The W_{du} is selected at a 10 % output peak overshoot for all models. The response parameter values for the models, namely LE, AE, and RR, are presented in Table 1. The optimisation algorithm used to select the W_{du} at 10 % output peak overshoot for each model is presented in Fig. 6. The output reference step response and the manipulated input (roots blower rpm) are shown in Fig. 12. This comparative analysis allows for a comprehensive understanding of the performance of each model under the same conditions, thereby facilitating the selection of the most effective model for real-time control strategy.

Table 1 shows comparative data using two control performance parameters for the LE, AE, and RR MPC systems using W_{du} weights selected at 10 % output reference step response peak percentage, including the control output reference step response rise time and the disturbance input step response peak percentage. The LE MPC system model exhibits the quickest reference step rise time at 20.7 s, indicating a faster response to changes in the reference value. On the other hand, the AE model shows the lowest disturbance input step peak at 6.8 %, suggesting a lower impact of disturbances on the system. However, the AE model's disturbance input step peak is lower than that of the LE model by about 2.3 %, while the reference step rise time of the AE model is almost double the LE model, with a difference of 19.3 s. The higher rise time indicates that the AE model takes longer to respond to changes in the reference value, which could be a critical factor in real-time control applications. Therefore, considering the balance between quick response time and moderate disturbance effect, the LE measure is the most suitable for this application. Its faster response time ensures that the system can quickly adapt to changes in the output reference. At the same time, its moderate disturbance effect means that the system is not overly sensitive to disturbances, making it a robust choice when dealing with unexpected changes in the real-time control environment.

3.3. Model predictive control near the pressure drop minimum curve

Case studies for the pneumatic conveying of plastic pellets were conducted to explore the proposed real-time model predictive control (MPC) system performance, as shown in Fig. 1. The real-time MPC control system is designed to optimise the Roots blower speed to achieve the desired largest Lyapunov exponent (LE) measure of the bottom arc-shaped electrostatic sensor and react when the flow is disturbed by changing the solids mass flow rate. This control system contains three subsystems: (i) open-loop control, (ii) sparse identification of nonlinear dynamics with control (SINDYc) model training and (iii) a closed-loop MPC. Each subsystem depends sequentially on the progression of the subsystems before it, starting with data collection using the open-loop control and ending with implementing the closed-loop MPC. Implementing the subsystems requires a user-defined input to switch between the open- and closed-loop control, parameters setting for each subsystem and three predefined functions for three variables: the manipulated input, disturbance input and output reference. The manipulated input is the Roots blower rpm, and the disturbance input is the solids mass flow rate, controlled using the rotary feeder speed and one output reference - the LE measure for the closed-loop MPC subsystem.

The pressure sensors data was collected at 4 Hz, while the bottom arc-shaped electrostatic sensor data was at 100 Hz and synced with the control inputs by adjusting the analysis measures moving data window step accordingly. The moving data window step to compute the analysis

Table 1
Control performance parameters of the LE, AE and RR control systems response to changes in their reference values.

Model output	LE	AE	RR
W_{du} selected at 10 % reference step response peak	12	19	16
Reference step response rise time	20.7 s	40.6 s	22.3 s
Disturbance input step response peak %	6.8 %	4.5 %	28.5 %

measures is set to 0.25 s to sync the LE time series with the pneumatic conveying system inputs. The LE measure parameters of electrostatic sensor data are considered to be in the same settings as the open-loop control system used to identify the MCAV described in Subsection 3.1.

The SINDYc model training subsystem parameters are the training dataset window size, SINDYc model identification parameters, number of models to store in the model database, model mean absolute error tolerance and checking frequency. The training dataset window size was set to 60s of data. The SINDYc model identification parameters are the library of candidate functions designed with polynomial multiplication functions of order one of all compensation between the manipulated input and output, the model accuracy and complexity balancing parameter $\varepsilon = 0.1$. The model database stores a maximum of 5 models. The mean absolute error tolerance was set to 5 %, where the error of the stored models was checked every 30s.

The parameters required to implement the real-time MPC subsystem are the control input horizon, the output prediction horizon, and the cost function weights, including state deviation, effort of input and effort of input rate of change (W_{du}). The control and prediction horizons were set to 1 s, the weight of state deviation = 1 and the weight of effort of input = 0. Two values for the W_{du} were considered for testing: 15 and 20.

Two case studies are presented below to provide insights into the dynamics and effectiveness of the proposed pneumatic conveying control system strategy. These case studies have different scenarios in which the pneumatic conveying system is subject to predefined functions and parameters to examine the performance of the real-time MPC system.

3.3.1. Case study 1: Reference and disturbance step response

This case study explores four real-time MPC pneumatic conveying experiments. The experiments are designed to examine the real-time control system's adaptability to changes in the LE reference value, the solids mass flow rate, and the MPC weight W_{du}, as documented in Table 2. The goal is to understand the system's response under varying conditions, particularly regarding air velocity. The LE is specifically targeted to reach a steady-state value near the MCAV range between 5.9 m/s to 8.75 m/s. The MCAV is a critical condition of this study as it is used to select the operating conditions at which the real-time control system response and ability to maintain stability were examined, as shown in Fig. 13 for experiments 1 and 2 and Fig. 14 for experiments 3 and 4.

In the first experiment, as shown in Fig. 13, the rotary feeder speed remains constant throughout the conveying process, maintaining a steady solids mass flow rate of 0.56 kg/s. For the first 30s, the pneumatic conveying open-loop control system was enforced by the Roots blower speed using a sinusoidal wave function with a period of 30s, centred at 1175 rpm, with lower and upper limits of 860 rpm and 1499 rpm, respectively. The closed-loop control was switched on, and the LE reference value started at a constant value of 39 for 30s. A step change is applied, reducing the LE reference value to 30 for the following 36 s. Subsequently, the LE reference value is returned to 39 for the next 35 s. The steady-state air velocity changes from 6.1 m/s to 19.1 m/s as the LE reference value decreases from 39 to 30. Before reaching the final steady state, the peak air velocity is 20 m/s, 2 % lower than the LE reference value, indicating a slight undershoot. The rise time for this experiment, with an MPC W_{du} of 15, is recorded as 5 s, as presented in Table 2.

The second experiment, illustrated in Fig. 13, follows a procedure similar to the first but with a W_{du} of 20. The steady-state air velocity decreases from 19.1 m/s to 6.1 m/s as the LE reference value increases from 30 to 39. Before reaching the final steady state, the peak air velocity remains at 19.1 m/s. The LE slightly undershoots with 1.12 %, similar to the first experiment. However, the rise time for this experiment is significantly longer and recorded as 17 s.

Fig. 14 shows the third and fourth experiments share the same LE reference and solids mass flow rate predefined functions but differ from the first two experiments. The difference between these two experiments is the MPC weight W_{du}, which is 15 in the third and 20 in the fourth

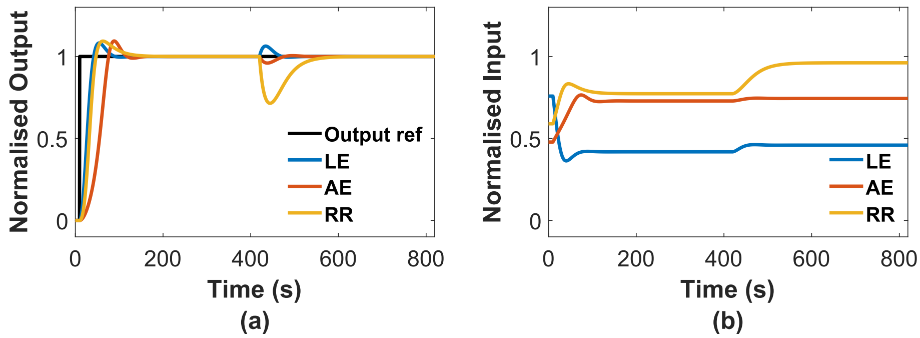

Fig. 12. (a) Normalised output response of the LE, AE, and RR system models to a step change in output reference. (b) Corresponding normalised manipulated input for each system model.

Table 2
The real-time LE control system response to changes in LE reference value at constant m_s and air velocity changes in m_s at constant LE reference.

	LE Reference				m_s Disturbance at LE = 34			
Step direction	Step down		Step up		Step down		Step up	
Step values	39 to 30		30 to 39		0.9 to 0.56 kg/s		0.56 to 0.9 kg/s	
Steady air velocity (m/s)	6.1 to 19.1		19.1 to 6.1		12.4 to 10.5		10.5 to 12.4	
MPC W_{du}	15	20	15	20	15	20	15	20
Rise time (s)	5	17	5	10		–		
Peak LE (% to ref)	− 2	− 1.12	+ 0.33	+ 0.3	− 11.7	− 20	+ 8.8	+5.8
Peak air velocity (% to ref)	+ 4.7	0	0	0	− 1.9	− 0.95	+ 20	+ 38

experiment. Following the open- to closed-loop control switch in the third experiment, the LE reference is set to a constant 34 throughout the conveying process. The rotary feeder rpm is set to maintain a continuous solids mass flow rate of 0.56 kg/s for 60s. The rotary feeder rpm is stepped up to change the mass flow rate to 0.9 kg/s for the following 61 s before returning to 0.56 kg/s for the final 35 s.

The steady-state air velocity decreases from 12.4 m/s to 10.5 m/s as the solids mass flow rate decreases from 0.9 kg/s to 0.56 kg/s to keep the LE constant. This response suggests that the system responds to a decrease in the solids mass flow rate by decreasing the air velocity. The peak air velocity before reaching the final steady state is 12.5 m/s. The measured LE undershoot was 11.7 % of the LE reference, indicating a significant undershoot. The rise time for this experiment, with an MPC W_{du} of 15, is 5 s.

In the fourth experiment, as shown in Fig. 14, a disturbance step is applied to the solids mass flow rate, from 0.56 kg/s to 0.9 kg/s at a constant LE of 34, but with an MPC W_{du} of 20. The steady-state air velocity increases from 10.5 m/s to 12.4 m/s as the solids mass flow rate increases from 0.56 kg/s to 0.9 kg/s at a constant LE of 34. This response indicates that the system responds to an increase in the solids mass flow rate by increasing the air velocity. The overshoot in the LE, as a percentage of the LE reference, is 5.1 %, while the peak air velocity before reaching the final steady state is 17.1 m/s. The rise time for this experiment is 10s.

3.3.2. *Case study 2: Reference sequential stepping with disturbance step response*

This section presents the results of the second real-time MPC case study, illustrated in Fig. 15. The scenario for this control experiment was designed to investigate the LE control system's response when operating near and below the MCAV. The control scenario starts with 10s of open-loop control to ensure an accurate model is selected and sent to the MPC. The closed-loop control was switched on, and a predefined LE reference function was initiated. This function was structured to take three upward steps in a sequence, with each step increasing the LE reference by 5.5, starting from a base value of 28. The LE reference was constant for 3.45 s during the first two steps and 4.5 s during the third step, reaching an LE of 44.5. This sequence was then mirrored with three downward steps, each decreasing the LE reference by 5.5, from 44.5 back to 28, with the same step time sequence. The value of 44.5 was chosen to operate the control system slightly below the MCAV, where the LE value was 44 at the minimum pressure drop point of 66 Pa/m, while the solids mass flow rate was 0.56 kg/s.

This sequence of three upward steps followed by three downward steps was repeated three times during the control experiment. The first sequence was applied at a constant solids mass flow rate of 0.56 kg/s, increased to 1 kg/s for the second sequence, and then decreased to 0.56 kg/s for the third sequence. Each sequence lasted 23 s, with changes in the solids mass flow rate.

During the experiment, there were three instances (Peak 1, 2, and 3) where the LE reference reached a maximum value of 44.5 and three instances (referred to as Trough 1, 2, and 3) with a minimum value of 28. The maximum measured LE and air velocity values for the three peak LE reference values were 45.5, 51.2, and 44.5, corresponding to 4.5 m/s, 5.1 m/s, and 5.8 m/s. The minimum measured LE values for the three trough LE reference values were 27.6, 27, and 27.7, with corresponding air velocities of 18.4 m/s, 20.5 m/s, and 19.1 m/s.

During Peak 1, where the LE reference value increased from 28 to 44.5 at a solids mass flow rate of 0.56 kg/s, the pressure drop in the horizontal pipeline reached an optimal minimum value of 66 Pa/m before increasing again. However, during Peak 2, where the LE reference value increased from 28 to 44.5 at a solids mass flow rate of 1 kg/s, the pressure drop reached a minimum value of 88.25 Pa/m before increasing again. As the LE reference sequentially retraced back from 44.5 to 28 during Trough 2, the pressure drop rapidly increased to a maximum of 330 Pa/m, a 37 % increase from the previous local pressure drop minimum. Concurrently, the LE value reached a maximum of 51.4. The control response in this situation was to increase the blower speed to decrease the LE value to the required lower LE reference value.

3.4. *General discussion*

The control studies conducted in Sections 3.1, 3.2 and 3.3 each serve a distinct purpose and are interconnected, ultimately leading to the final section on real-time model predictive control (MPC) case studies. These studies primarily revolve around the nonlinear dynamics analysis measures of electrostatic sensor data, including the largest Lyapunov exponent (LE), approximate entropy (AE), and recurrence rate (RR) and their relationship with three parameters, air velocity, pressure drop, and solids mass flow rate, in the open-loop control crossing the pressure minimum drop curve (PMC). The control of these measures has significant implications for optimising the pneumatic conveying of plastic

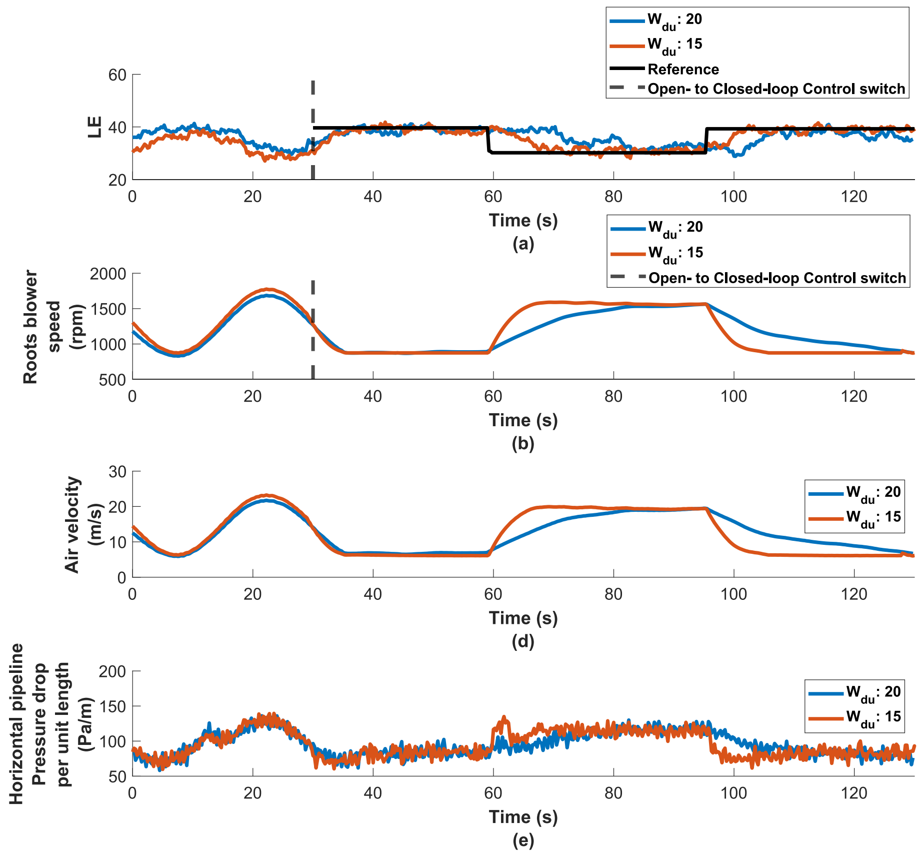

Fig. 13. Experimental data of two real-time LE MPC responses subjected to solids mass flow rate step up and down from 0.56 kg/s to 0.9 kg/s at a constant LE of 34, considering MPC cost function weight W_{du} of 20 and 15, including (a) the LE measured and reference and (b) Roots blower speed, and the horizontal pneumatic conveying states including (c) solids mass flow rate, (d) air velocity and (e) pressure drop per unit length of the horizontal pipeline vs time.

pellets. The objective is to operate near minimum energy consumption conditions at the PMC in the pneumatic conveying state diagram. The flow behaviour through the LE, AE, and RR above, near, and below the minimum conveying air velocity (MCAV) provides valuable insights. These three regions of operation at different MCAVs at different solids mass flow rates, the PMC points, are the focus of this discussion.

When operating across the MCAV condition, the LE measure exhibits an indirect relationship with the air velocity at different constant solids mass flow rates and directly with the solids mass flow rate at constant air velocity, as shown in Fig. 16 (a). Therefore, applying an MPC to manipulate the airflow using the blower to reach a desired LE reference value will increase the measured LE as the mass flow rate of solids increases. Subsequently, the air velocity will increase to drop the measured LE to the desired LE reference value. On the other hand, the AE and RR measures at constant solids mass flow rate and at air velocity higher than the MCAV have a direct relationship with the air velocity, as shown in Fig. 16 (b) and (c).

Near and below the MCAV, the AE correlates directly with air velocity. However, the RR shifts near the MCAV, reaching a minimum value, then below the MCAV condition, shifting to an inverse relationship with the air velocity. The unique behaviour of RR, particularly its shift near the MCAV and an inverse relationship with the air velocity below the MCAV, has significant implications for the control strategy. If an MPC is applied to manipulate the airflow using the blower to reach an RR reference value that decreases the air velocity across the MCAV, the RR value will decrease above the MCAV and increase again below the MCAV. Suppose the model used in the MPC does not incorporate this correlation (which means that if the model were not updated fast enough to know that the RR has a minimum value at the PMC, it will respond by decreasing the Roots blower speed and, subsequently the air velocity will decrease even further pushing the system to an unstable dense phase conveying mode.

Moreover, the RR has a strong direct relationship with the solids mass flow rate at constant air velocity, meaning that by applying an MPC to manipulate the airflow using the blower to reach a desired RR reference, the measured RR will increase as the mass flow rate of solids increases. Therefore, the air velocity will significantly increase to drop the measured RR to the desired RR reference value. On the other hand, the AE has a weak correlation with the solids mass flow rate. Hence, the air velocity slightly increased to maintain the AE value at the desired reference in the MPC setting. The strength in the increase or decrease of the air velocity with the solids mass flow rate as a response to maintaining a desired reference value for each of the LE, AE and RR models in MPC controllers, RR is higher than LE and AE. This leaves two stable control strategies across the PMC: applying MPC using models of LE and AE for their ability to control the system above, near and below the MCAV. According to the MPC simulation evaluation, the LE measure was selected based on its fast control response, precisely, rise time than the AE, and its response to an increasing solids mass flow rate makes it suitable for control across the PMC and its moderate distance effect.

This dynamic adjustment of the LE reference value and the corresponding control response demonstrates the adaptability of the real-time MPC system. The system's ability to operate near and below the MCAV while maintaining control and responding to changes in the solids mass flow rate is a significant achievement. Fig. 17 (a) and (b) depict the 3D state space of the pneumatic conveying system under real-time MPC, tracing the exact trajectories of system states: air velocity, solids mass flow rate, and pressure drop. The distinction lies in their colour bars: Fig. 17 (a), with the LE reference colour bar, and Fig. 17 (b), with the measured LE colour bar, represent the same points in the state space but

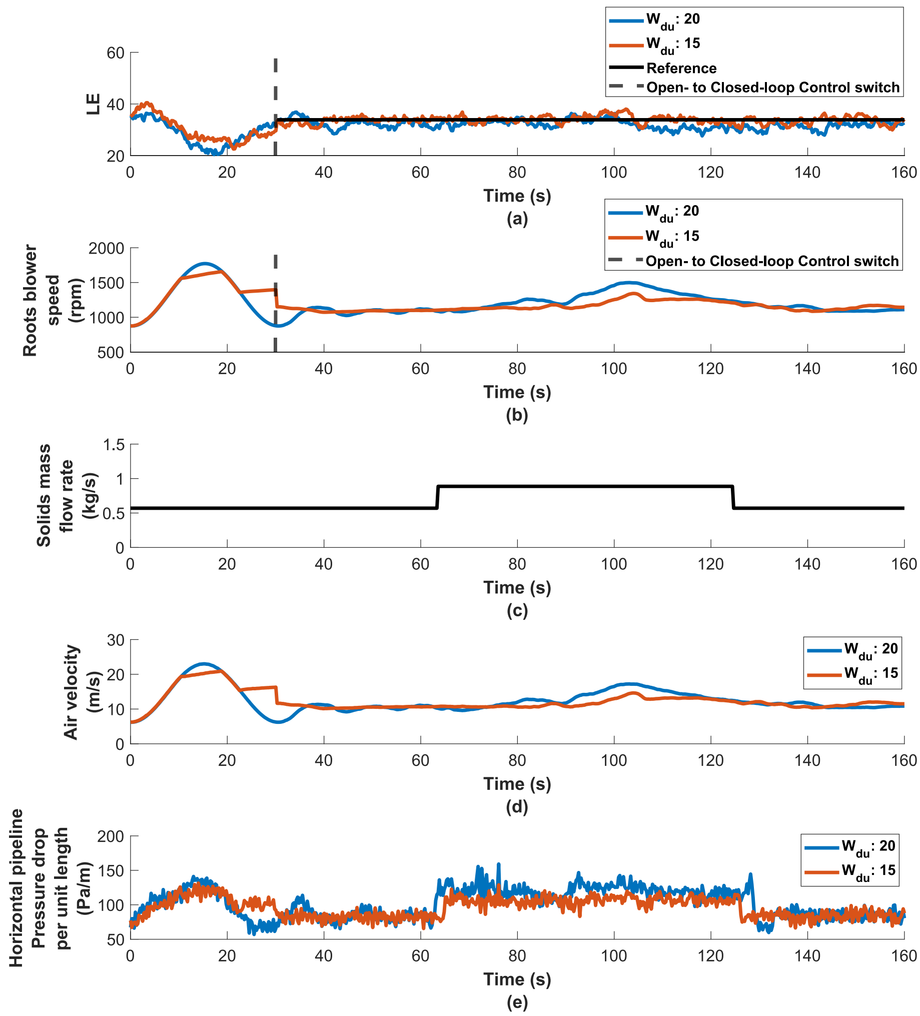

Fig. 14. Experimental data of two real-time LE MPC responses subjected to solids mass flow rate step up and down from 0.56 kg/s to 0.9 kg/s at a constant LE of 34, considering MPC cost function weight W_{du} of 20 and 15, including (a) the LE measured and reference and (b) Roots blower speed, and the horizontal pneumatic conveying states including (c) solids mass flow rate, (d) air velocity and (e) pressure drop per unit length of the horizontal pipeline.

with different colour spectrums. These figures demonstrate how the LE reference values can effectively guide the pneumatic conveying system state towards a desired operating condition.

In the first sequence, the system successfully navigated the LE reference from 28 to 44.5 and back to 28 at a solids mass flow rate of 0.56 kg/s. The pressure drop reached an optimal minimum, indicating efficient operation. However, the second sequence, conducted at a higher solids mass flow rate of 1 kg/s, presented a more challenging scenario. Despite the increased solids mass flow rate, which will increase the minimum pressure drop, the system could still navigate the LE reference values effectively. This suggests the system can handle variations in solids mass flow rate while maintaining control near the PMC. The third sequence, which returned to the initial solids mass flow rate of 0.56 kg/s, further demonstrated the system's robustness. Despite the rapid increase in pressure drop and the LE value during the downward stepping sequence, the system responded effectively by increasing the rpm, thereby reducing the LE value to the required lower reference value. This showcases the LE MPC system's ability to react to disturbances in the solids mass flow rate and adjust the Roots blower speed accordingly.

4. Conclusions

This research focused on modelling and controlling the gas-solid flow in the pneumatic conveying of plastic pellets to achieve minimum energy consumption operation. The study was structured in three main stages; each successive stage was developed on the findings of the previous one.

Initially, an open-loop pneumatic conveying control system was developed. This system was essential for collecting input-output data while operating at various conditions: above, near, and below the minimum conveying air velocity (MCAV). Insights were gained into the flow behaviour using nonlinear dynamics analysis measures of the electrostatic sensor data, critically near the MCAV. Specifically, the open-loop experiments identified the MCAV as being in the air velocity range of 5.9 to 8.75 m/s, where the pressure drop reached a minimum of 68.2 Pa/m. Electrostatic sensor data confirmed that the largest Lyapunov exponent (LE) decreased with air velocity above MCAV, while approximate entropy (AE) and recurrence rate (RR) measures exhibited a direct relationship with air velocity. These findings provided crucial data for subsequent model development.

In the second stage, the data from the open-loop control system was used to identify models with the sparse identification of nonlinear dynamics with control (SINDYc). These models were then tested within a model predictive control (MPC) simulation framework. This step helped to understand the MPC performance and its response to different disturbances. Based on these evaluations, a suitable nonlinear analysis method was selected and integrated into a closed-loop control system using an MPC combined with SINDYc. The MPC simulation framework demonstrated that the LE model exhibited the most responsive control

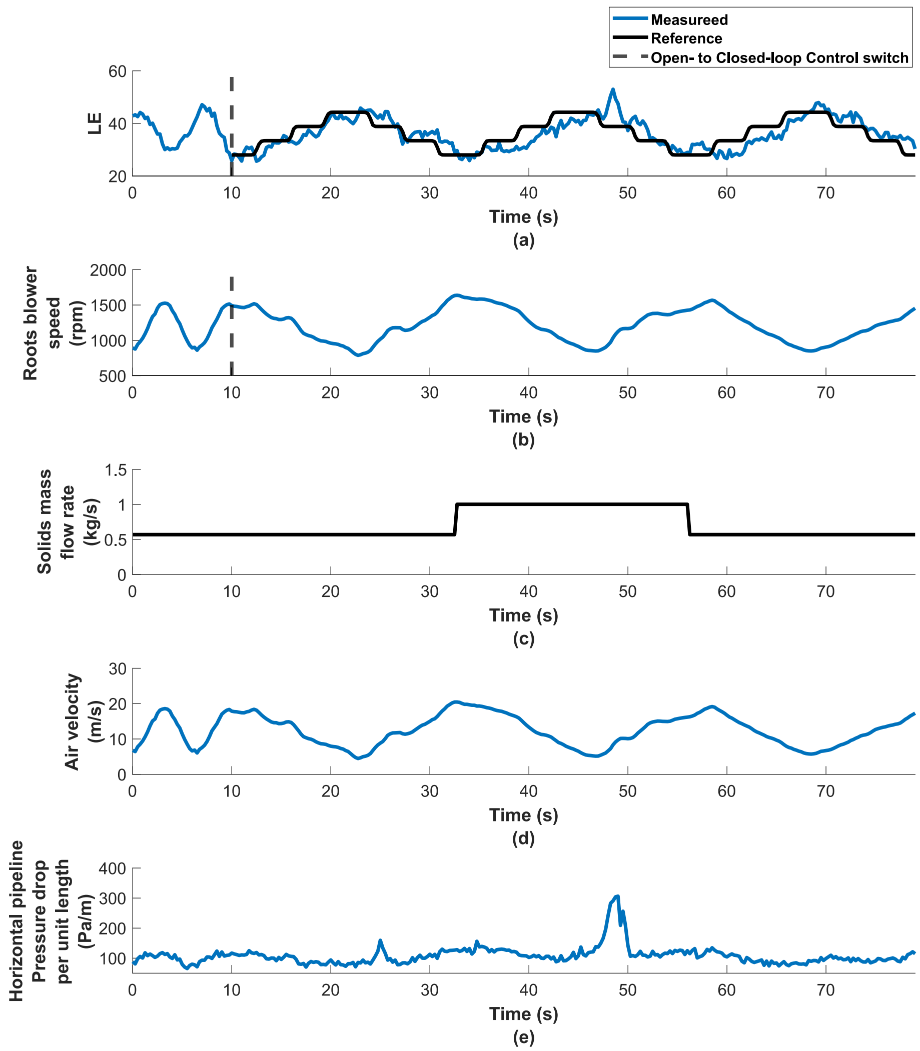

Fig. 15. Experimental data of the real-time LE MPC responses subjected to LE reference sequential stepping up and down from 28 to 44.5 and solids mass flow rate step up and down from 0.56 kg/s to 1 kg/s, including (a) the LE measured and reference and (b) Roots blower speed, and the horizontal pneumatic conveying states including (c) solids mass flow rate, (d) air velocity and (e) pressure drop per unit length of the horizontal pipeline.

performance, with a rise time of 20.7 s and only a 6.8 % disturbance peak. This made it the most suitable model for real-time control, showing robustness in handling varying airflow and solids mass flow rates while maintaining system stability.

The final stage involved the real-time application of the MPC near the MCAV. Several real-time MPC control case studies were conducted to assess the control performance of a selected system model when operating near the MCAV condition. This allowed for identifying areas for improvement and studying the effects of different control parameters. The case studies showed that controlling near the pressure minimum curve (PMC) with an LE reference resulted in stable control of air velocity and pressure drop. The system maintained optimal performance by adjusting the blower speed in response to changes in solids mass flow rate. A critical outcome was the ability of the control system to maintain a stable LE reference while navigating dynamic solids mass flow rates near and below the pressure drop minimum curve (PMC). The system exhibited effective real-time control, maintaining the LE within the desired range, even during rapid step changes in the solids mass flow rate. In Case Study 2, despite an increased solids mass flow rate (0.56 kg/s to 1 kg/s), the system responded by effectively reducing the Roots blower speed to adjust the air velocity and maintain a low pressure drop. This dynamic response led to an increase in pressure drop by 37 % during downward LE stepping, which was mitigated by an increase in the blower speed, demonstrating the robustness of the system in controlling LE across varying flow conditions, particularly near the MCAV.

This research offers a data-driven approach to identify and control the pneumatic conveying process. It also highlights the benefits of using chaos and recurrence quantification analysis for energy-efficient systems. In particular, the integration of LE, AE, and RR into the control strategy allowed for fine-tuned real-time control, enabling the system to operate efficiently across a wide range of conditions. This study highlights the unique behaviour of the RR below MCAV, where it shifts to an inverse relationship with air velocity, marking a key insight into flow dynamics that future control systems can leverage. The three interconnected studies emphasise the importance of a comprehensive approach to understanding and controlling complex systems. The general discussions further elaborated on the contributions and implications of each stage. The findings demonstrate that adaptive control using MPC and nonlinear dynamics can lead to significant energy savings and operational stability, even under highly dynamic conditions near the MCAV. It is strongly believed that the findings from this research will be pivotal for designing energy-efficient pneumatic conveying systems and related areas.

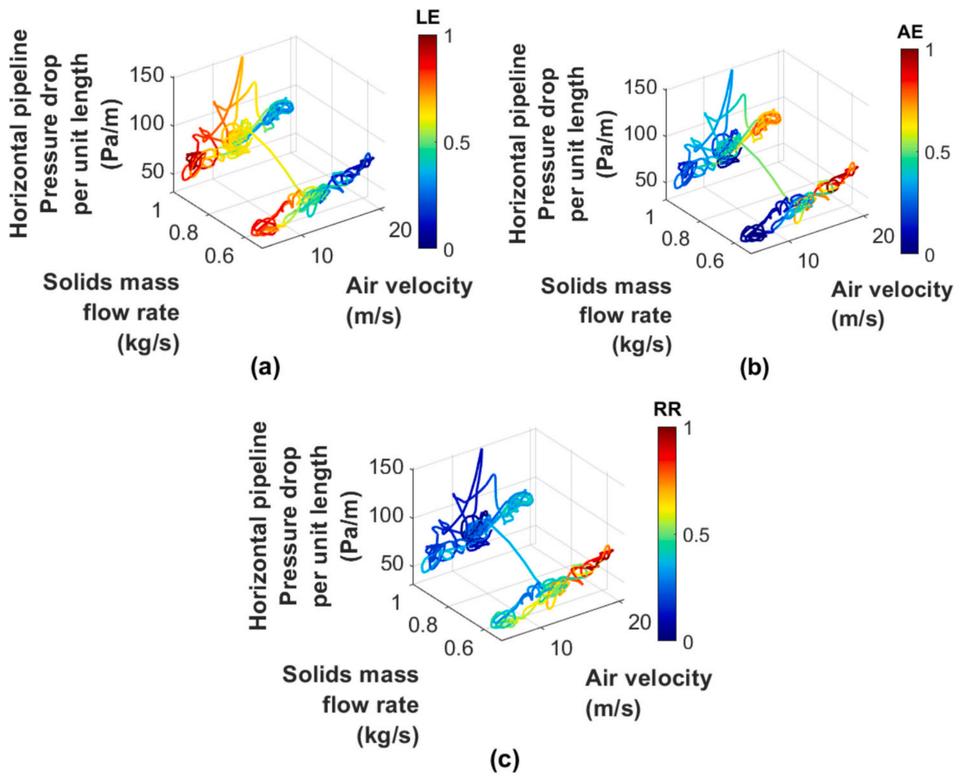

Fig. 16. 3D state spaces of the pneumatic conveying system, including air velocity, solids mass flow rate and moving mean pressure drop per unit length of the horizontal pipeline with 4 points (2 s) window, correlated with normalised (a) LE, (b) AE and (c) RR, enforced by the Roots blower speed.

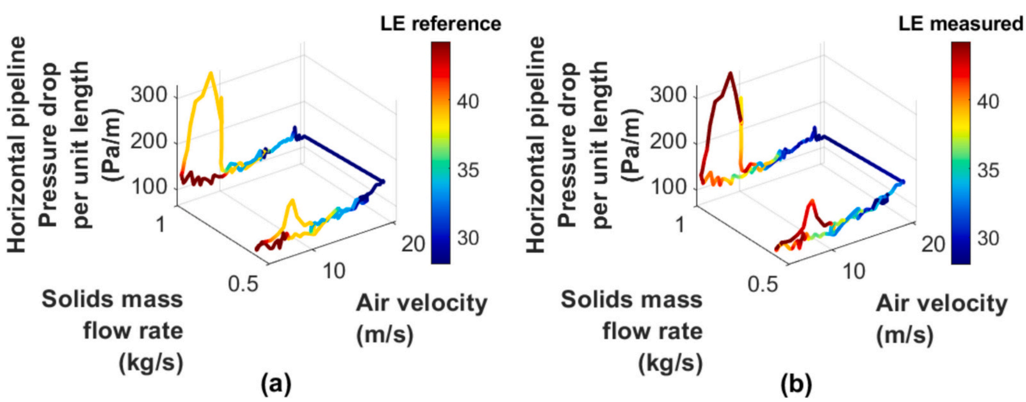

Fig. 17. A 3D state space of the pneumatic conveying system under real-time MPC, tracing system state trajectories of air velocity, solids mass flow rate, and pressure drop of the horizontal pipeline, guided by LE reference values towards desired operating conditions, where the colour bar in (a) is the reference and (b) the measured LE.

List of symbols

MCAV	Minimum conveying air velocity, m/s
PMC	Pressure drop minimum curve, Pa/m
$P_{1,\ \mathrm{Blower\ exit}}$	Pressure sensor taping at blower exit
P_2 to P_4	Pressure sensor tapings in horizontal pipeline
t	Time, s
x(t)	Data point value at specific, t
τ	Time delay
m	Embedding dimension
n	Number of data points
N	Number of phase points
$Y(t)$	Phase space (Time series vector)
i and j	Subscript for phase points indexes
r	Radius of a hypersphere
$\Theta(h)$	Heaviside step function
s	Subscript for nearest neighbour phase point index
k	Subscript for Expansion step index
k_{Min}	Minimum expansion step
k_{Max}	Maximum expansion step
dt	Time difference between acquired data points
$\lambda(i)$	Lyapunov exponent
LE	Largest Lyapunov exponent
Φ	Statistical function
AE	Approximate entropy
r	Radius hypersphere threshold
RR	Recurrence rate
$\frac{\mathrm{dX}}{\mathrm{dt}}$	Derivative of state vector with respect to time
X and U	State and input data vector
Θ	Library of candidate functions

$\Xi(\xi)$	Matrix of sparse coefficients
ε	Parameter for balancing accuracy with complexity in sparse identification of nonlinear dynamics with control
W_x	Optimisation weight for state deviation
W_u	Optimisation weight for effort of input
W_{du}	Optimisation weight for effort of input rate of change
H_c	Control horizon
H_p	Prediction horizon

CRediT authorship contribution statement

Osamh S. Alshahed: Writing – review & editing, Writing – original draft, Visualization, Validation, Software, Project administration, Methodology, Investigation, Formal analysis, Data curation, Conceptualization. **Baldeep Kaur:** Writing – review & editing, Visualization, Validation, Supervision, Project administration, Methodology, Investigation, Formal analysis, Conceptualization. **Michael S.A. Bradley:** Writing – review & editing, Visualization, Validation, Supervision, Resources, Project administration, Methodology, Investigation, Formal analysis, Conceptualization. **David Armour-Chelu:** Writing – review & editing, Visualization, Validation, Supervision, Formal analysis.

Declaration of competing interest

The authors declare that they have no known competing financial interests or personal relationships that could have appeared to influence the work reported in this paper.

Data availability

Data will be made available on request.

Acknowledgements

The author would like to acknowledge the financial support from the University of Greenwich through the Vice-Chancellor scholarship (VCS-ES-04-19) and technical support from the entire team at The Wolfson Centre for Bulk Solids Handling Technology, University of Greenwich.

References

[1] D. Mills, Pneumatic Conveying Design Guide, Third Edit, Butterworth-Heinemann, 2016, https://doi.org/10.1016/C2014-0-02678-0.
[2] A.E. Kabeel, M. Elkelawy, H.A.E.D. Bastawissi, A.M. Elbanna, An experimental and theoretical study on particles-in-air behavior characterization at different particles loading and turbulence modulation, Alex. Eng. J. 58 (2019) 451–465, https://doi.org/10.1016/j.aej.2019.04.002.
[3] G. Klinzing, F. Rizk, R. Marcus, L.S. Leung, Pneumatic Conveying of Solids: A Theoretical and Practial Approach, Third edit, Springer, 2010, https://doi.org/10.1007/978-90-481-3609-4.
[4] A. Levy, H. Kalman, Handbook of Conveying and Handling of Particulate Solids, First edit, Elsevier, 2001.
[5] P.W. Wypych, J. Yi, Minimum transport boundary for horizontal dense-phase pneumatic conveying of granular materials, Powder Technol. 129 (2003) 111–121, https://doi.org/10.1016/S0032-5910(02)00224-3.
[6] A.K. Saha, D. Das, R. Srivadtava, P.K. Panigrahi, K. Muralidhar, Fluid Mechanics and Fluid power - Contemporary Research, 2016, https://doi.org/10.1007/978-81-322-2743-4.
[7] K.C. Williams, Dense Phase Pneumatic Conveying of Powders: Design Aspects and Phenomena, The University of Newcastle, 2008.
[8] R. Pan, Material properties and flow modes in pneumatic conveying, Powder Technol. 104 (1999) 157–163, https://doi.org/10.1016/S0032-5910(99)00044-3.
[9] Y. Tsuji, Y. Morikawa, S. Sugimotc, S.I. Miyoshi, Y. Nakano, Flow pattern and pressure fluctuation in air-solids two-phase flow in a pipe at low velocities, Int. J. Multiphase Flow 48 (1982) 656–663, https://doi.org/10.1299/kikaib.48.656.
[10] S.V. Dhodapkar, G.E. Klinzing, Pressure fluctuations in pneumatic conveying systems, Powder Technol. 74 (1993) 179–195, https://doi.org/10.1016/0032-5910(93)87010-L.
[11] G.A. Jama, G.E. Klinzing, F. Rizk, Analysis of unstable behavior of pneumatic conveying systems, Part. Sci. Technol. 17 (1999) 43–68, https://doi.org/10.1080/02726359908906805.
[12] J.B. Pahk, G.E. Klinzing, Assessing flow regimes from pressure fluctuations in pneumatic conveying of polymer pellets, Part. Sci. Technol. 26 (2008) 247–256, https://doi.org/10.1080/02726350802028926.
[13] J.S. Shijo, N. Behera, Transient parameter analysis of pneumatic conveying of fine particles for predicting the change of mode of flow, Particuology 32 (2017) 82–88, https://doi.org/10.1016/j.partic.2016.07.004.
[14] A. Kumar, T. Deng, M.S.A. Bradley, Application of arc-shaped electrostatic sensors for monitoring the flow behaviour at top and bottom section of a pneumatic conveying pipeline, Measurem. Sens. 10–12 (2020) 1–8, https://doi.org/10.1016/j.measen.2020.100026.
[15] C. Wang, L. Jia, W. Gao, Electrostatic sensor for determining the characteristics of particles moving from deposition to suspension in pneumatic conveying, IEEE Sensors J. 20 (2020) 1035–1042, https://doi.org/10.1109/JSEN.2019.2945572.
[16] O.S. Alshahed, B. Kaur, M.S.A. Bradley, D. Armour-Chelu, Application of nonlinear dynamics analysis to gas-solid flow system in horizontal pneumatic conveying of plastic pellets, Powder Technol. 428 (2023) 118837, https://doi.org/10.1016/j.powtec.2023.118837.
[17] S.L. Mckee, T. Dyakowski, R.A. Williams, T.A. Bell, T. Allen, Solids flow imaging and attrition studies in a pneumatic conveyor, Powder Technol. 82 (1995) 105–116, https://doi.org/10.1016/0032-5910(94)02894-T.
[18] T. Suppan, M. Neumayer, T. Bretterklieber, S. Puttinger, H. Wegleiter, A model-based analysis of capacitive flow metering for pneumatic conveying systems: a comparison between calibration-based and tomographic approaches, Sensors 22 (2022), https://doi.org/10.3390/s22030856.
[19] F. Takens, Detecting strange attractors in turbulence dynamical systems and turbulence, Dynam. Syst. Turbul. 898 (1981) 366–381, https://doi.org/10.1007/bfb0091924.
[20] Bidinger Maiti, Nonlinear Time Series Analysis, Second edi, The Press Syndicate of the University of Cambridge, 2004.
[21] J.P. Eckmann, O. Oliffson Kamphorst, D. Ruelle, Recurrence plots of dynamical systems, Europhys. Lett. 4 (1987) 973–977, https://doi.org/10.1209/0295-5075/4/9/004.
[22] J.P. Zbilut, C.L. Webber Jr., Embeddings and delays as derived from quantification of recurrence plots, Phys. Lett. A 171 (1992) 199–203, https://doi.org/10.1016/0375-9601(92)90426-M.
[23] H. Ji, H. Ohara, K. Kuramoto, A. Tsutsumi, K. Yoshida, T. Hirama, Nonlinear dynamics of gas-solid circulating fluidized-bed system, Chem. Eng. Sci. 55 (2000) 403–410, https://doi.org/10.1016/S0009-2509(99)00335-8.
[24] N. Ellis, L.A. Briens, J.R. Grace, H.T. Bi, C.J. Lim, Characterization of dynamic behaviour in gas-solid turbulent fluidized bed using chaos and wavelet analyses, Chem. Eng. J. 96 (2003) 105–116, https://doi.org/10.1016/j.cej.2003.08.017.
[25] M.F. Llop, N. Jand, K. Gallucci, F.X. Llauró, Characterizing gas-solid fluidization by nonlinear tools: chaotic invariants and dynamic moments, Chem. Eng. Sci. 71 (2012) 252–263, https://doi.org/10.1016/j.ces.2011.12.031.
[26] Y. Zhou, X. Zhu, T. Qi, Fractal characteristic analysis of multi-source information of gas-solid two-phase flow in a riser, J. Chem. Eng. Jpn 50 (2017) 476–484, https://doi.org/10.1252/jcej.16we203.
[27] Y. Lu, P. Kang, L. Yang, X. Eric Hu, H. Chen, R. Zhang, Y. Jeffrey Zhou, X. Luo, J. Wang, Y. Yang, Multi-scale characteristics and gas-solid interaction among multiple beds in a dual circulating fluidized bed reactor system, Chem. Eng. J. 385 (2020), https://doi.org/10.1016/j.cej.2019.123715.
[28] B. Babaei, R. Zarghami, H. Sedighikamal, R. Sotudeh-Gharebagh, N. Mostoufi, Investigating the hydrodynamics of gas-solid bubbling fluidization using recurrence plot, Adv. Powder Technol. 23 (2012) 380–386, https://doi.org/10.1016/j.apt.2011.05.002.
[29] M. Tahmasebpour, R. Zarghami, R. Sotudeh-Gharebagh, N. Mostoufi, Characterization of various structures in gas-solid fluidized beds by recurrence quantification analysis, Particuology 11 (2013) 647–656, https://doi.org/10.1016/j.partic.2012.08.005.
[30] M.F. Llop, N. Gascons, Multiresolution analysis of gas fluidization by empirical mode decomposition and recurrence quantification analysis, Int. J. Multiphase Flow 105 (2018) 170–184, https://doi.org/10.1016/j.ijmultiphaseflow.2018.04.006.
[31] F.J. Cabrejos, G.E. Klinzing, Characterization of dilute gas-solids flows using the rescaled range analysis, Powder Technol. 84 (1995) 139–156, https://doi.org/10.1016/0032-5910(95)02980-G.
[32] F.J. Cabrejos, G.E. Klinzing, Pickup and saltation mechanisms of solid particles in horizontal pneumatic transport, Powder Technol. 79 (1994) 173–186, https://doi.org/10.1016/0032-5910(94)02815-X.
[33] F. Fu, M. Kong, C. Xu, C. Liang, S. Wang, Flow characterization of dense-phase pneumatic conveying system of pulverized coal through electrostatic sensor arrays, Adv. Mech. Eng. (2013) 1–12, https://doi.org/10.1155/2013/656194.
[34] S. Wang, C. Xu, J. Li, Z. Ding, S. Wang, An instrumentation system for multi-parameter measurements of gas-solid two-phase flow based on capacitance-electrostatic sensor, Measurement 94 (2016) 812–827, https://doi.org/10.1016/J.MEASUREMENT.2016.09.010.
[35] K. Miyazaki, G. Chen, F. Yamamoto, J.I. Ohta, Y. Murai, K. Horii, PIV measurement of particle motion in spiral gas–solid two-phase flow, Exp. Thermal Fluid Sci. 19 (1999) 194–203, https://doi.org/10.1016/S0894-1777(99)00020-5.
[36] R. Deloughry, E. Pickup, Investigation of the closed-loop control of a pneumatic conveying system using tomographic imaging, Process Imag. Autom. Control 4188 (2001) 103, https://doi.org/10.1117/12.417155.
[37] B. Satpati, C. Koley, S. Datta, Sensor-less predictive drying control of pneumatic conveying batch dryers, IEEE Access 5 (2017) 3547–3568, https://doi.org/10.1109/ACCESS.2017.2675625.

[38] B. Satpati, C. Koley, P.S. Bhowmik, S. Datta, Nonlinear model predictive control of pneumatic conveying and drying process, in: 2014 IEEE Conference on Control Applications, CCA. Part of 2014 IEEE Multi-Conference on Systems and Control, MSC 2014, Institute of Electrical and Electronics Engineers Inc., 2014, pp. 492–497, https://doi.org/10.1109/CCA.2014.6981394.

[39] Katsuhiko Ogata, Modern Control Engineering, Prentice-Hall, 2010.

[40] H.C.T. Thu, M. Lee, Analytical design of proportional-integral controllers for the optimal control of first-order processes with operational constraints, Korean J. Chem. Eng. 30 (2013) 2151–2162, https://doi.org/10.1007/s11814-013-0153-1.

[41] J.N. Juang, R.S. Pappa, An eigensystem realization algorithm for modal parameter identification and model reduction, J. Guid. Control. Dyn. 8 (1985) 620–627, https://doi.org/10.2514/3.20031.

[42] G.E.P. Box, G.M. Jenkins, G.C. Reinsel, G.M. Ljung, Time Series Analysis: Forecasting and Control, 2015.

[43] H. Peng, J. Wu, G. Inoussa, Q. Deng, K. Nakano, Nonlinear system modeling and predictive control using the RBF nets-based quasi-linear ARX model, Control. Eng. Pract. 17 (2009) 59–66, https://doi.org/10.1016/j.conengprac.2008.05.005.

[44] T. Zhang, G. Kahn, S. Levine, P. Abbeel, Learning Deep Control Policies for Autonomous Aerial Vehicles with MPC-Guided Policy Search. http://arxiv.org/abs/1509.06791, 2015.

[45] M.O. Williams, I.G. Kevrekidis, C.W. Rowley, A data–driven approximation of the Koopman operator: extending dynamic mode decomposition, J. Nonlinear Sci. 25 (2015) 1307–1346, https://doi.org/10.1007/s00332-015-9258-5.

[46] M. Krishnan, S. Gugercin, P.A. Tarazaga, A wavelet-based dynamic mode decomposition for modeling mechanical systems from partial observations, Mech. Syst. Signal Process. 187 (2023), https://doi.org/10.1016/j.ymssp.2022.109919.

[47] E. Kaiser, J.N. Kutz, S.L. Brunton, Sparse identification of nonlinear dynamics for model predictive control in the low-data limit, in: Proceedings of the Royal Society A: Mathematical, Physical and Engineering Sciences 474, 2018, https://doi.org/10.1098/rspa.2018.0335.

[48] D.P. Bertsekas, Model predictive control and reinforcement learning: a unified framework based on dynamic programming, IFAC-PapersOnLine 58 (2024) 363–383, https://doi.org/10.1016/j.ifacol.2024.09.056.

[49] M.T. Rosenstein, J.J. Collins, C.J. De Luca, A practical method for calculating largest Lyapunov exponents from small data sets, Phys. D 65 (1993) 117–134, https://doi.org/10.1016/0167-2789(93)90009-P.

[50] S.M. Pincus, Approximate entropy as a measure of system complexity, Proc. Natl. Acad. Sci. USA 88 (1991) 2297–2301, https://doi.org/10.1073/pnas.88.6.2297.

[51] J.P. Eckmann, O. Oliffson Kamphorst, D. Ruelle, Recurrence plots of dynamical systems, Europhys. Lett. 4 (1987) 973–977, https://doi.org/10.1209/0295-5075/4/9/004.

[52] C.L. Webber, J.P. Zbilut, Dynamical assessment of physiological systems and states using recurrence plot strategies, J. Appl. Physiol. 76 (1994) 965–973, https://doi.org/10.1152/jappl.1994.76.2.965.

[53] R. Tibshirani, Regression shrinkage and selection via the lasso, Source J. Royal Stat. Soc. Ser. B (Methodol.) 58 (1996) 267–288. https://www.jstor.org/stable/2346178 (accessed August 15, 2023).

[54] S.L. Brunton, J.L. Proctor, J.N. Kutz, W. Bialek, Discovering governing equations from data by sparse identification of nonlinear dynamical systems, Proc. Natl. Acad. Sci. USA 113 (2016) 3932–3937, https://doi.org/10.1073/pnas.1517384113.

[55] J.O. Flower, G.F. Knott, S.C. Forge, Application of Schroeder-phased harmonic signals to practical identification, Measurem. Control 11 (1978) 69–73, https://doi.org/10.1177/002029407801100204.